Application of the Mesoporous Silica Nanoparticles for the Controlled Delivery of TNF-alpha as Immune Therapy

Dissertation

Zur Erlangung des Grades

“Doktor der Naturwissenschaften”

Im Promotionsfach Chemie

am Fachbereich Chemie, Pharmazie und Geowissenschaften der

Johannes-Gutenberg-Universität

vorgelegt von

Kimia Rahmani

geboren in AHVAZ, IRAN

Mainz 2022

Eidesstattliche Versicherung

This dissertation was written independently and without any unauthorised help. It was the author's responsibility to ensure that all textual passages that are appropriated verbatim or paraphrased from published and unpublished sources are properly listed and cited according to bibliographical standards. In carrying out this research, I complied with the rules of standard scientific practice as formulated in the statutes of the Johannes Gutenberg-Universität Mainz to insure standard scientific practice.

Kimia Rahmani

Mainz 2022

Everything you can see in the universe is pretty much just empty space

ZUSAMMENFASSUNG

Mesoporöse Silica-Träger (spezifisch hinsichtlich Porenstruktur und -durchmesser) wurden für den Tumor-Nekrose-Faktor-α (TNF-α) Beromun hergestellt, um eine maximale Verkapselungseffizienz zu erreichen. Das Verhältnis von TNF-α Beromun zu Silica-Träger wurde optimiert. Die Verkapselungseffizienz für TNF-α Beromun mit kleinporigen Dendrimer-analogen mesoporösen Silica-Trägern ist mit 30 % für kleine Porenweiten immer geringer als mit 96 % für große Porenweiten. Die mesoporösen Silica-Träger wurden mit einem Poly-l-Lysin Polymer verkapselt, um zu analysieren, wie ein organischer Hilfsstoff, der die Freisetzung von TNF-α kontrolliert, den endosomalen Abbau beeinflusst. Eine kontrollierte/zellspezifische Freisetzung von TNF-α konnte erzielt werden. Dies ist für die immuntherapeutische Behandlung von Hautkrebs essentiell.

Die Eignung der Formulierung aus mesoporösen Silica-Trägern, gezielt dendritische Zellen (DCs) zu adressieren, internalisiert zu werden und die T-Zellen zu aktivieren, wurde in vitro anhand von Markern der DC-Aktivierung und über die Expression costimulatorischer Moleküle charakterisiert und optimiert. Für unbeschichtete und mit TNF-α beladene mesoporöse Silica-Träger wurde eine starke Reifung der DCs und eine starke Proliferation von T-Zellen nachgewiesen. Im Gegensatz dazu wurde für TNF-α-beladene Silica-Partikel, die Poly-l-Lysin beschichtet waren, innerhalb von 48 Stunden keine Reifung von DCs und keine Proliferation von T-Zellen beobachtet, was auf eine erfolgreiche Polymer-Beschichtung schließen lässt.

SUMMARY

In an effort to control immune responses purposefully, a specific mesoporous silica carrier was synthesised for tumour necrosis factor-α (TNF-α) Beromun (regarding pore structure and diameter), to achieve a maximum encapsulation efficiency with an optimum concentration of the mesoporous silica carrier. The encapsulation efficiency for TNF-α Beromun with small pore dendrimer-like mesoporous silica nanocontainers is always lower (30%) for small pores than for large pores (96%). The mesoporous silica nanocontainers were encapsulated with an amino acid-based polymer (poly-l-lysine) to demonstrate how the nature of a polymer that controls release can impact endosomal degradation. A controlled and cell specific release of TNF-α was achieved, which is promising for skin cancer treatment by stimulating adaptive immune resistance.

The ability of the mesoporous silica nanocontainer formulation to target dendritic cells (DCs), become internalised, and activate the T cells was characterised and optimised in vitro using markers of DCs activation and costimulatory molecules. Strong maturation of DCs and proliferation of T cells was shown for uncoated silica carriers loaded with TNF-α. In contrast, no maturation of DCs and no T cell proliferation was observed for poly-l-lysine coated TNF-α loaded particles within 48 hours indicating successful polymer coating.

Contents

1. Introduction

1.1. Nano-delivery and targeting systems in nanomedicine and challenges in the clinical translation

As a form of medical treatment, nanomedicine employs nanotechnology to diagnose, prevent, and treat diseases using highly specific therapies. The most discussed aspects of nanotechnology are drug loading, stability and storage, complexity of nanocarriers, characterization challenges for nanopharmaceuticals and toxicity.[1] Researchers, universities, governments and industries have paid much attention to the use of nanotechnology for medical purposes over the past ten years.[2–4] It is challenging to determine the relationship between critical quality attributes and efficacy, since the regulatory environment and perceptions are changing continuously. As long as such approaches can be delivered cost-effectively, the advantages should not be overlooked.[3]

An aspect of nanomedicine that has garnered a lot of attention is nanoparticle (NP) drug delivery (nanoparticles that contain drug molecules) typically accomplished by parenteral administration. Besides delivering drugs through numerous mechanisms including solubilisation, passive and/or active targeting, and triggered release, nanoparticle drug delivery systems (DDSs) seek to enhance their therapeutic index (increase their encapsulation efficacy and/or reduce their toxicity). Especially if these compounds degrade easily in biological environments, nanoencapsulation offers the opportunity to protect and to solubilise them, e.g., to deliver compounds with physicochemical properties that strongly limit their aqueous solubility and therefore systemic uptake.[5,6] By targeting drug delivery and triggering release the behaviour of drug molecules becomes more predictable, so they are delivered more efficiently to the target site, which is one approach to achieve high therapeutic index. In parallel, it has led to a reduced accumulation of toxic substances in many healthy body sites.[7]

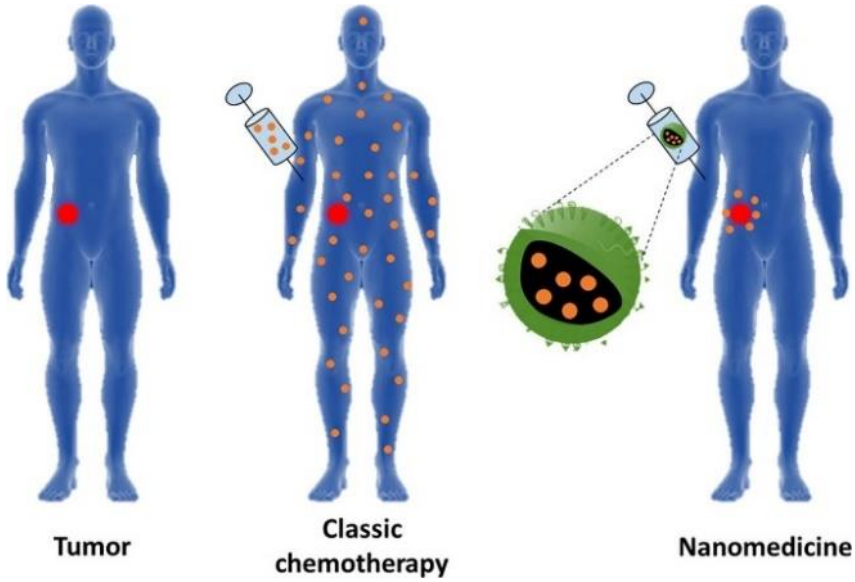

Figure 1. **Classic chemotherapy versus nanoparticle drug delivery**. Adapted with permission from ref. [7].

However, despite a multitude of proof-of-concept clinical results, nanoparticle DDSs have not successfully translated into clinical practice as rapidly as might have been expected given the number of positive preclinical results.[8] Unlike conventional formulation technology, which contains free drug, integrating multiple components into a single nanosized carrier requires several chemical procedures and several formulation processes. The multiple steps inevitably lower the yield and increase the cost of production.[1] In most FDA-approved cases, nanodrugs are derived from conventional drugs that were already approved and they are comprised of only simple NPs.[9] A number of other factors are at play here too; the efficacy of drugs in animal models does not necessarily translate into human efficacy, since the delivery of drugs within the human body varies a great deal especially when treating diseases. Biologically, it is crucial to understand how nanomedicine interacts with tumour microenvironment and cellular/intracellular compartments in vivo.[3] It is also very important from a chemical viewpoint to be able to obtain proper comparison between similar systems and to avoid exaggerated differences between them (reproducibility).[10] Nevertheless, in the near future, pharmaceutical nanomedicine will play a major role in the worldwide pharmaceutical market and healthcare system, and a clear trend is the shift from relatively simple nanoparticles originating from traditional materials categories to complex and multi-component materials that blur the boundaries between organic/inorganic chemistry and molecular biology.[9,11]

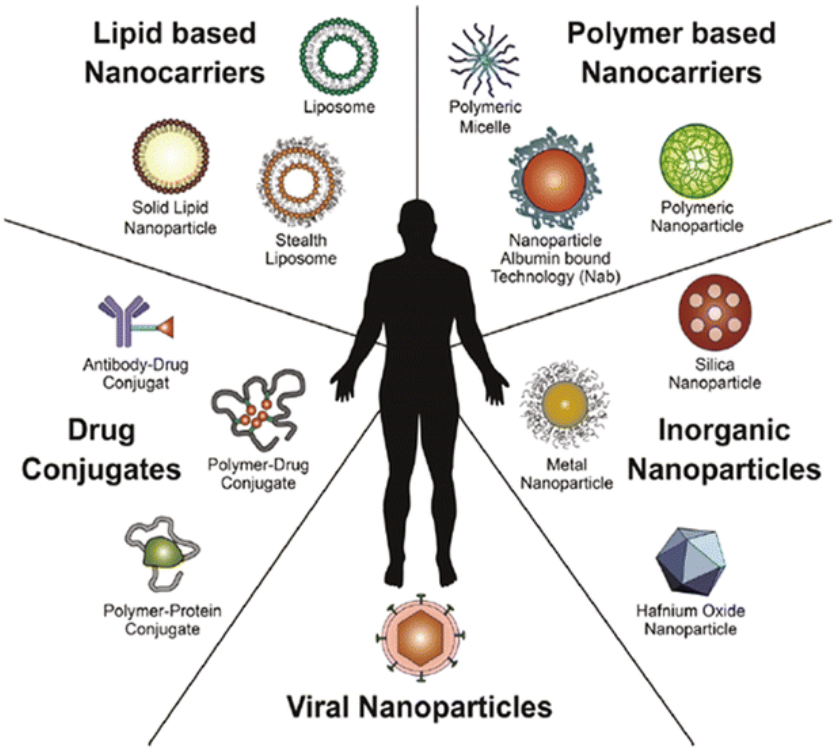

Figure 2. **Overview of established nanomedicines in the clinic**. This diagram shows an overview of the nanomedicines currently being investigated in the clinic for cancer treatment. Lipid-based, polymer-based, inorganic, viral, and drug-conjugated nanoparticles are examples of platforms that have been established in clinical research. With permission from ref. [12].

2. Literature discussion

2.1 Current status of biological therapies for the treatment of metastatic melanoma (The development of TNF-α-MSN formulations in this PhD thesis will belong to the biological immune therapeutics for the treatment of skin cancer).

Biological therapy for cancer is a type of treatment that uses the body's immune system to kill cancer cells and is used in the treatment of many types of cancer to prevent or slow tumour growth and to prevent the spread of cancer. Biological therapy for cancer often causes fewer toxic side effects than do other cancer treatments.

“Melanoma is a highly aggressive skin cancer arising from the malignant transformation of melanocytes residing in the basal layer of the epidermis. Although early stage surgical excision can reach a 5-year survival rate over 95%, the prognosis for advanced stage, metastatic disease remains extremely poor as the overall incidence and mortality associated with melanoma continues to rise on an epidemiological scale. Traditional chemotherapies, generally aimed at inhibiting cell division, have historically shown little survival benefit. This has led to changes in treatment approaches over the preceding two decades as contemporary methods for the treatment of advanced or metastatic melanoma now involve a number of biological modalities, which include immunotherapeutic approaches, targeted therapies and epigenetic modification therapies”.[13]

2.2 Interaction between nanoparticles and human dendritic cells

Dendritic cells (DCs) originally “discovered by Ralph Steinman and Zanvil Cohn in 1973 are professional antigen presenting cells (APCs)”, essentially capable of proliferating and differentiating naive T cells in their mature phases.[14,15] Differentiated from monocytes, immature DCs in peripheral tissues digest antigens, retrieve their antigenic information, and present it on their surfaces, in combination with major histocompatibility complex (MHC) molecules.[16] The transfer from immature to mature phase (phenotype) through pathogen-associated molecular patterns (PAMPs) or danger-associated molecular patterns (DAMP), is accompanied by morphological and functional changes.[15,17] A maturing DC loses its adhesive structure, modifies its

cytoskeleton, becomes highly mobile and establishes the migration path to lymphoid organs.[18]

Antigens can be internalised by endocytosis or phagocytosis. During their journey from early endosomes or phagosomes to lysosomes, they undergo gradual proteolytic degradation. The whole process of trafficking from early compartments to lysosomes might destroy potentially important peptide epitopes for T-cell activation.

“DCs maturation also leads to a decrease in their endocytic activity but increased expression of MHC-II and co-stimulatory molecules.[14] However, recent studies show that endocytosis and phagocytosis are actually only slowed down or slightly decreased in mature DCs. It has observed that fully mature DCs still take up considerable amounts of antigen, particulate, or soluble.[19] Mature DCs express higher levels of the chemokine receptor, CCR7 and secrete cytokines, essential for T-cell activation. Thus, the interaction between mature DCs and antigen-specific T cells is the trigger of antigen-specific immune responses. When interacting with CD4+ T cells, DCs may induce their differentiation into different T helper (Th) subsets such as Th1, Th2, Th17, or other CD4+ T cell subtypes”.[14]

As an experimental tool, human peripheral blood monocyte-derived DCs (mo-DCs) have been extensively used due to the practical difficulties in studying tissue DCs. Plus, an in vivo equivalent of mo-DCs may be seen in inflammatory tissue rather than healthy tissue.[20]

There is a plethora of materials used in the development of DCs-targeting nanomedicines for both activation and suppression of immune responses. These materials must fulfil three main requirements: They must be (i) biocompatible, (ii) non-toxic and (iii) easy to manipulate in size, shape and surface chemistry. Promising results have been obtained with nanoformulations made of organic materials such as liposomes,[21,22] polymers including poly(lactic-co-glycolic acid) (PLGA), polylactide, poly(β-amino esters) and polyethylene glycol (PEG),[23–25] or inorganic materials including Au,[26,27] porous silicon (pSi),[28,29] and mesoporous silica nanoparticles (MSN).[30] The bulk material forming the nanoparticles is important because it may itself influence the development of subsequent immune responses. Some materials have certain properties that can make them immunogenic, which make these materials ideal carriers for vaccines, but equally undesirable if the goal is to induce tolerance.[31] To

conclude this part, in vitro and in vivo study on DCs activation were conclusive in showing that minor differences in the chemical composition and protein affinity (entrapped or adsorbed) in the developed NP had an extensive impact on their uptake and activation of DCs.[32]

Immature DCs actively sample their local environment for antigens, and they are able to take up a wide range of exogenous materials such as viruses, bacteria and other particulates *via* a variety of internalization mechanisms.[33] Nanoparticles with a diameter under 100 nm can be effectively internalised by clathrin-mediated endocytosis,[23] and DCs are also capable of internalizing larger material *via* phagocytosis or micropinocytosis. Nanoparticle size may not prove to be a critical parameter in terms of uptake as nanomaterials ranging from a few nanometres up to more than a micrometre have been documented to be successfully internalised by DCs.[33,34] However, nanoparticle size is important in dictating the transport kinetics of the antigen, affecting the ability of nanoparticles to drain to the lymph nodes and induce an adaptive immune response.[34] This transport to the lymph nodes has been found to be restricted to nanoparticles with a diameter under 200 nm, allowing them to reach lymph-node-resident DCs for antigen presentation within hours of injection.[34–36] Nanoparticles larger than 200 nm either reach the lymph nodes through migratory DCs, which after internalizing nanoparticles—most likely in the blood, spleen, liver or injection site—traffic to the lymph nodes and/or remain at the injection site.[34] As a result, direct antigen processing by DCs within the lymph nodes through small nanoparticles could lead to early T cell activation, which might result in an enhanced adaptive response compared to the one achieved from migratory DCs transporting larger nanoparticles.[37]

By fine-tuning nanoparticle size, interactions with other immune cell populations could also be minimised given the differences in biodistribution and lymph drainage of nanoparticles.[38] Nanoparticles with virus-like sizes (20–200 nm) have a higher propensity to interact with B cells [34] as free-draining nanoparticles may predominantly access B cell-resident areas within the lymph nodes. Conversely, larger nanoparticles are more likely to remain in the interstitial space before entering the lymphatics with an increased chance to be phagocytosed by barrier cells—mainly DCs and macrophages. Moreover, virus-like particles (<200 nm) are likely to be eliminated

faster by the liver given their tendency to associate with liver sinusoidal endothelial cells, instead of APCs.[39]

Similarly, morphology influences not only the way DCs recognise nanoparticles but also the characteristics of the subsequent immune response and should be considered together with size.[40] Niikura et al.[41] reported that spherical, rod-like and cubic Au nanoparticles with the same surface chemistry and protein loading generated different profiles of cytokine secretion in APCs, with differing antibody titres following vaccination in mice. The former could not be explained solely through differential uptake, suggesting that DCs may be able to distinguish nanoparticles based on their morphology. Rod-like nanoparticles elicited a pro-inflammatory response possibly due to lysosomal rupture—suggesting that nanorods have a greater potential as adjuvants to elicit immunity rather than tolerance. However, the influence of the nanoparticle geometry may well be size dependent, with different immune responses observed depending on the size range of the differently shaped nanoparticles.[40] Nevertheless, drawing distinct conclusions between these different studies is challenging, as there are a number of differences in the experimental set-up and analysis. Multiple parameters can be normalised for example, keeping total antigen dosage[40] or total surface area[41] which can influence the findings.

Additionally, the nanoparticle surface properties are vital, since cells, tissues, and media detect and interact with particles on their surface. Different surface modifications of nanoparticles can affect their interaction and internalization into DCs. In a biological setting, proteins can adsorb onto NPs surface—known as a protein corona—based on their surface chemistry,[42,43] which can typically lead to aggregation or macrophage uptake. An example of the later are immunoglobulins (IgGs) which are involved in the general process of opsonization.[44] Moreover, studies have shown that cationic nanoparticles are more prone to be internalised by cells, including DCs. Fytianos et al. studied the uptake, pro-inflammatory effects and immunological response in DCs of Au nanoparticles (15 nm) with different surface functionalities (PEG, PVA (polyvinyl alcohol) and a mixture of both) and charge (positive and negative). They demonstrated that positively charged PVA–Au nanoparticles had an increased DCs uptake and a more prominent necrotic effect.[26] The significant decrease in cell viability of positively charged PVA–Au nanoparticles was not observed in the PEGylated counterparts, suggesting that cytotoxicity depends on the

combination of both the nanoparticle surface chemistry and charge. Other studies have also shown that PVA-coated nanoparticles can induce increased co-stimulatory molecules and activation of DCs, suggesting a preference of immunity over tolerance. In addition, slower uptake by DCs was observed when nanoparticles were coated with the antigen on the surface as opposed to those loaded into the particle interior.[32]

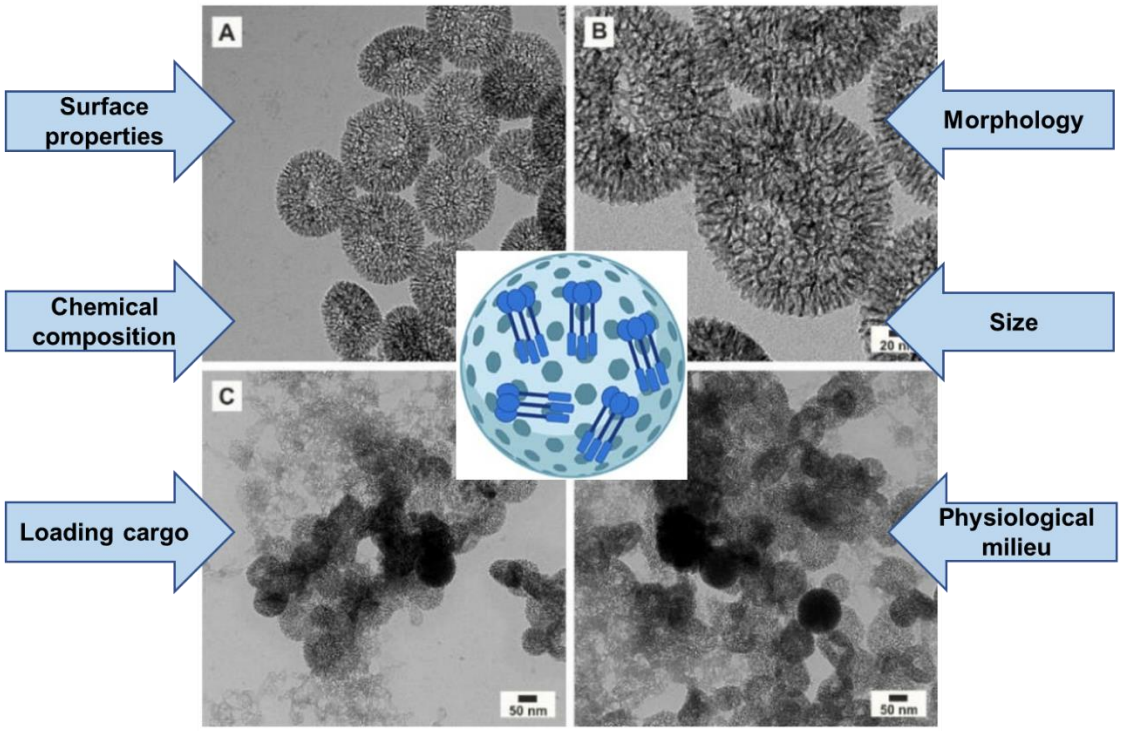

Figure 3. **Principal factors affecting nanoparticles´ fate in physiological environment.** TEM images are adapted from Sven Kurch´s thesis[45]: (A,B) after 48h, (C,D) after 7 days.

2.3 Mesoporous silica nanoparticles (MSNs) as drug delivery and targeting system

The reasons for the interest on nanoparticles and, specifically, on MSNs for drug delivery according to a review of Vallet-Regí et al.[46] first and most importantly relays on the scale of MSNs interaction with living systems. It is well known that human cells present a broad size variability, but most of them are normally in the micrometre range. That scale similarity between MSNs and cells would present an intimate interaction. Secondly, MSNs allow a fine control over the pharmacokinetic profile of the transported therapeutic agent. The use of MSNs as controlled drug delivery systems could keep the drug concentration at optimal levels over prolonged periods of time,

improving the efficiency of the treatment and avoiding any type of potential toxicity and the subsequent side effects. Thirdly, the great loading capacity of MSNs allows transporting two or more drugs into the same nanoparticles, which allows designing combined therapies for tackling multiresistant tumours. The scale-up of the synthesis of MSNs is not trivial, because many different factors must be considered during synthesis. MSNs are often developed in the lab, where milligrams or grams of product are obtained, but the production of large-scale batches under good manufacturing practice (GMP) conditions, which are needed for preclinical screening, clinical trials and clinical use, is a roadblock for their commercialization.

Croissant and co-workers showed in their review that silica and organosilica have controllable morphology, composition, porous structure and pore size, surface chemistry, and dispersibility.[47]

Yang and colleagues outlined their research progress on silica-based controlled drug delivery systems, including a) pure mesoporous silica sustained-release systems, b) magnetism and/or luminescence functionalised mesoporous silica systems to integrate targeting and tracking properties of drug molecules, and c) stimuli-responsive controlled release systems, which adapt their release to environmental changes, such as pH, redox potential, temperature, photoirradiation and biomolecules.[48]

The questions to be addressed are: What would be the ideal particle characteristics (size, morphology, drug loading strategy, degradability, etc.) for clinical use? Which drug delivery mechanism would be ideal? And finally, how could silica NPs better benefit patients when compared to other clinically approved nano vectors? Many of these questions remain largely unanswered empirically to date and should therefore be the focus of future research.[47,49,50]

Mesoporous silica nanoparticles with pore sizes of 2–50 nm have beneficial properties, such as a large surface area (>1000 m^2/g), making them an ideal platform for diagnosis and as vehicles for drug or gene delivery. Compared with organic nanoparticles, silica nanoparticles have a considerably higher loading capacity, particularly for biologics, good mechanical stability, and they can be tuned to control drug release in response to internal (for example, pH, enzyme and bacteria) and/or external (for example, pH, light, heat and magnetic field) stimuli.[51]

Silica nanoparticles also possess self-adjuvant properties, which is desirable for the development of next- generation nano vaccines.[50] Consequently, silica nanoparticles with good safety, efficacy, degradability and viability may be applicable in more diverse clinical scenarios than their organic counterparts.

Published results on the preparation of DMSN in combination with a pH sensitive cationic hyperbranched polyethyleneimine (PEI) hydrophilic polyethylene glycol (PEG) copolymer gatekeeper and its use for the encapsulation of TNF-α have shown low encapsulation efficiency and low reproducibility of the preparation and application of PEI-PEG polymer.

Kienzle, Kurch et al.[52] have shown that DMSN, in combination with a pH sensitive PEI-PEG copolymer gatekeeper, can be used for encapsulation and shielding of a highly toxic cargo for cancer treatment, such as the TNF-α homotrimer Beromun. They used 3D fluorescent ubiquitination-based cell cycle indicator (FUCCI) spheroids that efficiently mimic tumour architecture and microenvironment and confirmed that DMSN penetrated these spheroids and after release from DMSN, TNF-α induced G1 cell cycle arrest and subsequently cell death in a time and dose-dependent manner.

The focus of the current work is to develop, optimise and investigate an in vitro MSN delivery system that meets the following requirements for a translation into the preclinical and clinical development of TNF-α nanomedicine for activation of adaptive immunity:

I. High yield of the MSN production
II. High encapsulation efficiency
III. Easy and robust coating using commercially available polymers
IV. Investigating the impact of coated and uncoated loaded-NPs on activation of adaptive immunity

Mesoporous silica nanoparticles with extra-large pores/ ultra-large cavity can be used as an attractive platform for large proteins delivery and cancer vaccines.[53,54]

Among the impressive number of polymers reported in literature so far, the commercial hyperbranched poly-l-lysine (mol wt 15,000-30,000) has been chosen solely as a gatekeeper model, since the polycationic nature of this poly(amine)-based polymer at physiological pH is appropriate to cellular adhesion, endocytosis, and intracellular trafficking for therapeutic delivery.[55,56]

2.4 Synthesis and characterization of DMSNs

Contrary to MCM-41, which has hexagonally uniform channels of pores, DMSNs are complex to prepare, and conventional soft-templating methods are inadequate to address the complex dynamic self-assembly of negative silicate species and surfactants at the molecular level. This project selected micro-emulsion templating approach (MET) as the synthesis method for DMSNs with a centred radial pore orientation.

Because of the variety and ease of control, the substructures of microemulsions were used as templates to control the synthesis of mesoporous silica materials with different morphologies and mesostructures. In 2008, Okuyama[57] and coworkers first reported the synthesis of spherical mesoporous silica particles with a tunable pore size and tunable outer particle diameter in the nanometre range in a water/oil phase using the cationic surfactant CTABr as a template. This method involves the simultaneous hydrolytic condensation of tetraethylorthosilicate to form silica and polymerization of styrene into polystyrene (PS) in the presence of octane as the oil phase, and subsequent removal of PS by high temperature calcination in air resulted in the formation of DMSNs with large pores, where PS beads act as hard templates. By varying the conditions of the dispersed phase, e.g., the ratio of octane/water, the styrene concentration, the pH, and the temperature, during preparation, the pore size (4–15 nm) and grain diameter (20–80 nm) of the prepared MSNs can be precisely tuned. However, further research performed by Holmberg[58] suggested that the MSNs synthesised under the same conditions free of styrene possessed the same mesostructures, indicating that the polystyrene (PS) beads formed by polymerization of styrene were not the only template for the formation of DMSNs with large pores. In turn, the authors concluded that the microemulsion spontaneously formed at the interface of water and oil played the main role in controlling the formation of DMSNs with hierarchical pores.

Later, Zhao[59] and his collaborators developed a new biphase stratification approach for the synthesis of novel 3D-DMSNs with multigenerational and hierarchical dendrimer-like radially-centred mesopore channels, and it was also successfully expanded to prepare uniform core–shell mesoporous structures with varied functional cores (such as Au nanoparticles and Ag nanotubes) and 3D-dendritic mesopore radial

channels. In this report, a sophisticated interfacial emulsion driven self-assembly mechanism was proposed to explain the nucleation and growth process of DMSNs. Very recently, in the final collected sample, Xu[53] and coworkers found the presence of isolated cone-shaped structures, which could be used as building subunits to assemble DMSNs, whose shape was reminiscent of the funnel-like shape in the model of the biphase stratification approach. It is importantly noted that both groups commented that the final mesostructure of DMSNs was sensitive to the stirring rate of reaction media as discussed by Dang et al.[60], which indicates the rationality of the MET mechanism.

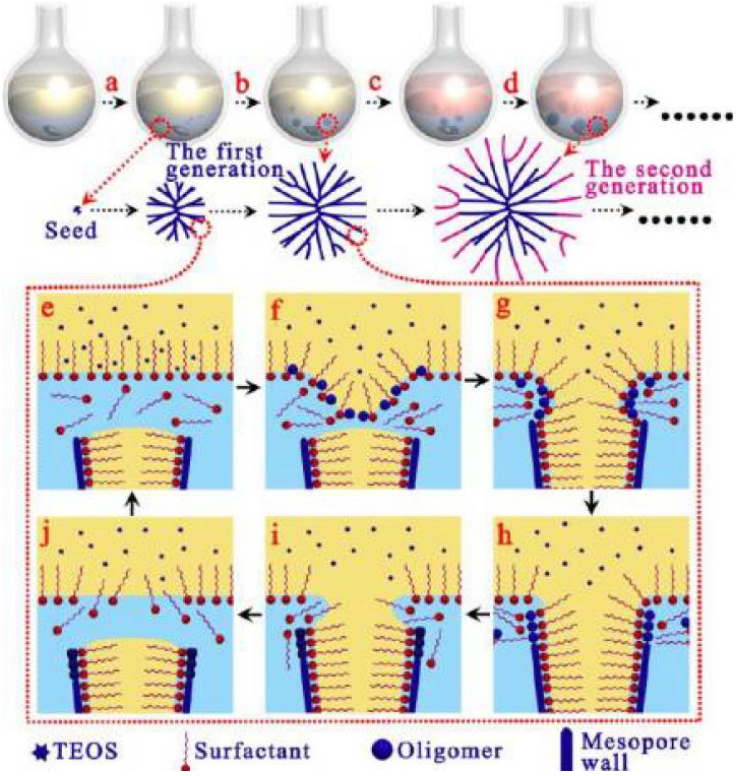

Figure 4. Synthesis process of the 3D-dendritic MSNSs and the mechanism of interfacial growth. (a) Nucleation process of the 3D-dendritic MSNSs; (b) growth process of the first generation of the 3D-dendritic MSNSs; (c) changing the upper oil phase; (d) growth process of the second generation of the 3D-dendritic MSNSs; (e−h) the mechanism of one single mesopore-channel growth with swelling. Adapted from [59].

2.5 Tumour necrosis factor-alpha (TNF-α) and interaction with dendritic cells

TNF-α (tumour necrosis factor alpha) is a cell signalling protein (cytokine) involved in systemic inflammation and is one of the cytokines that make up the acute phase reaction. It is produced chiefly by activated macrophages, although it can be produced by many other cell types such as $CD4^+$ lymphocytes, NK cells, neutrophils, mast cells, eosinophils, and neurons.[61] TNF-α is a member of the TNF superfamily, consisting of various transmembrane proteins with a homologous TNF domain. The primary role of TNF-α is the regulation of immune cells. Being an endogenous pyrogen, it can induce fever, apoptotic cell death, cachexia, inflammation and to limit tumorigenesis and viral replication and respond to sepsis via IL1 and IL6 producing cells.

Dysregulation of TNF-α production has been implicated in a variety of human diseases including Alzheimer's disease,[62] depression,[63] autoimmune[64] and inflammatory bowel disease (IBD).[65] Recombinant TNF-α is used as an immunostimulant under the name of INN-Tasonermin.

Beromun 1mg/5mL powder and solvent for solution is the first tumour necrosis factor to receive marketing approval. The protein consists of three identical polypeptide chains of 157 amino acids combined to form a compact, bell-shaped homotrimer. Each of the individual subunits have a relative molecular mass of 17350 Daltons. We can simply extract the TNF net charge at pH 7.4 using the protein sequence: (z=-23.91/Prot pi). The active substance is Tasonermin (tumour necrosis factor alfa -1a) which is produced by recombinant DNA technology in *Escherichia coli*. Beromun is indicated in adults as an adjunct to surgery for subsequent removal of the tumour to prevent or delay amputation, or in the palliative situation, for irresectable soft tissue sarcoma (STS) of the limbs, used in combination with melphalan *via* mild hyperthermic isolated limb perfusion (ILP). The systemic application of Tasonermin is limited by its acute toxic effects, the effective dose predicted from preclinical studies being substantially higher than the observed human maximum tolerated dose.[66]

There is substantial evidence that TNF-α affects both, activation and proliferation of different subsets of immune cells in many disease states. Maney et al.[67] have explored the mechanism by which TNF-α controls the maturation and survival of human DCs ('inflammatory' moDCs and steady-state blood CD1c+ DCs) through its two receptors, TNFR1 and TNFR2. They have shown that TNF-α mediated phenotypical maturation

of human DCs is, overall, most potently regulated by TNFR1, whereas DCs survival can be significantly enhanced by both TNFR. Thus, their data show that TNF-α promotes DCs maturation and survival through distinct signalling pathways, demonstrating that innate signals enhancing DCs survival do not necessarily result in enhanced DCs maturation.

Fully mature DCs exhibit high and homogeneous expression of CD83, CD80, CD86, MHC class-I and class-II analysed by flow cytometry. Functional testing is required as well. For this, alloreactive T cells are stimulated with different ratios of mature DCs. Half maximal T cell proliferation provoked by fully matured DCs is achieved at DC:T cell ratios of approximately 1:200".[68]

2.6 A glance at encapsulation and release principle

Over the past decade, encapsulation has been extensively explored in the pharmaceutical industry. Following active molecule encapsulation, biodistribution would no longer be related to the drug itself but to the carriers´ physicochemical properties.[69] Drug encapsulation as the best approach through employing biodegradable polymers may provide the biocompatible, easily administered, safe, comfortable and inert drug delivery system. Indeed, delivery systems possessing such properties could be defined as an ideal drug delivery system.[70]

The following content is partially taken and adapted from the book "Strategies to Modify the Drug Release from Pharmaceutical Systemschapter by Marcos Bruschi chapter main mechanisms to control the drug release":[71]

"There are chemical and biological mechanisms to control the drug release spatially. Basically, they are dissolution, diffusion, osmosis, partitioning, swelling, erosion, and targeting. It is common for a system or device to present more than one of them. The classification of controlled drug delivery systems regarding the mechanism of release is based on the main mechanism.

Dissolution: The human or animal organism consists mainly of water, and the drug needs to be dissolved in this fluid to be released from the system and exert the therapeutic effect. Therefore, the dissolution is a very important mechanism that can control the drug delivery. The dissolution process occurs when the solvating medium surrounding a solid drug particle is not saturated, the surface of solid contacts the

medium and the molecules are solvated and removed from the solid. The solvated molecules (solute) increase in the medium, increasing the concentration of solute. This increase of solute concentration produces a boundary layer around the solid where the dissolution medium tends to be saturated and the dissolution rate (dC/dt) decreases. The removal of the boundary layer causes the renewing of the solvent, increasing the dissolution rate. Thus, the difference between the solute concentration at the inner portion of the boundary layer (C1) and the outer boundary layer (C2) predicts the dissolution rates. When the difference is big, the dissolution rate is greater. However, when the difference is small, the dissolution rate is lower. The thickness of the boundary layer (l) is also important and conversely proportional to the dissolution rate. Considering the thickness of the boundary layer and the difference of solute concentration in the medium (inner and outer boundary layers), the dissolution rate may be described as: (diffusivity coefficient of solute= D, the surface area of solid= A)

$$\frac{dC}{dt} = \frac{D.A}{l}.(C_1 - C_2)$$

It is very important to note that the dissolution rate depends on the particle size, agitation and the viscosity of the dissolution medium, as well as the temperature. In this context, solubility is a thermodynamic property of an active agent and a medium. However, the dissolution rate is a kinetic property. The solubility coefficient of the drug in the medium decreases with the increasing melting point of the drug, and it increases with increasing chemical compatibility of the drug with the surrounding medium.

Partitioning: The drug partitioning in the medium is an important characteristic that influences the control of the drug release. Delivery systems can be constituted by one or more groups of materials displaying different affinities or polarities (e.g., hydrophilic and hydrophobic) and leading the active agent to the organism. This affinity can be measured by the ratio of drug solubilities in the two phases and is defined as partition coefficient:

$$P = \frac{C_o}{C_w},$$

where C_o is the concentration of the drug in the oil or hydrophobic phase and C_w is the concentration in the aqueous or hydrophilic phase.

Diffusion: Diffusion is defined as the process of mass transfer of individual molecules of a substance from one part of a system to another, carried by random molecular motions (thermal or Brownian motion), and is associated to forces such as concentration gradient. It is the process by which a concentration difference is reduced by a spontaneous flux of matter. This mass transfer at the system/water interface plays an important role in diffusion. The random molecular motions are also the cause of heat transfer by conduction, and there is an obvious analogy between the two processes. Assuming diffusing spherical particles or molecules, the relationship between its radius and diffusion coefficient is given by the Stokes–Einstein equation:

$$D = \frac{RT}{6\pi\eta r N_A}$$

where R is the general constant of gases (8.314 J mol^{-1} K^{-1}), T the temperature (K), η the viscosity (Pa s), r is the radius of the particle or molecule, and N_A is Avogadro's number (6.02×10^{23} mol^{-1}).

Erosion: The polymers used in drug delivery systems controlled by diffusion possess a relatively passive function. They are carriers and delay the rate with which the active agent is distributed to the targeting site. Some polymeric carriers are elaborated to play a more active function on the drug delivery process. These polymers suffer erosion when they suffer chemical reactions, releasing the active agent. For implantable or injectable therapies, these systems are popular because they do not require retrieval after the active agent is fully released. However, the erosion products must be non-toxic and excretable or resorbable.

The nature of the erosion mechanism can be provided by the hydrophilicity and morphology of the polymer. Hydrophobic polymers tend to exclude water from the interior of the system, and they will erode from the outer to inner portion of the system. On the other hand, hydrophilic polymers favour homogeneous erosion, and the crystallinity grade also has an influence on the process once the crystalline regions of polymer tend to exclude water with more intensity than the amorphous region.

Osmosis: Over the past 50 years, the application of one of the most fundamental principles of biology, osmosis, in a technical device, has enabled the control of the drug release rate. Drug delivery systems based on the principles of osmosis have been proposed as an effective manner to control the release rate. They are well

established, trusted systems that enable a wide range of applications, from oral dosage forms providing less than 24 h of release to implantable devices that precisely control the release of the active agent over periods of months, years or more. Moreover, the osmosis principle can be used together with other mechanisms to control the drug release rate.

Osmosis may be defined as the action in which the solvent is transferred through a semipermeable membrane to dilute a solution containing solute (also called osmolytes) and solvent. When two solutions of different concentrations are separated by a semipermeable membrane that is permeable to the smaller solvent molecules but not to the large solute molecules, then the solvent will tend to flow through the semipermeable membrane from the less concentrated to the more concentrated solution. It is an effort to equalise concentrations of the impermeable solutes on both sides of the membrane.

The solvent in biological systems is water. The transport of water and other molecules across biological membranes is essential to many processes in living organisms. Osmotic pressure is the energy that drives the process and controls the drug release from therapeutic systems. The rate of water transport through the membrane can be written as follows:

$$\frac{dV}{dt} = \left(\frac{A}{h}\right) k\Delta\pi$$

where dV/dt is the volume flow of solvent through the membrane, A is the cross-sectional area for transport, h is the membrane thickness, k=L p σ as the effective permeability of the membrane, Lp is the hydraulic permeability of the membrane, σ is the reflection coefficient and Δπ is the osmotic pressure difference across the membrane.

The coating of individual drug particles with semipermeable polymers can also control the drug release. When these particles are exposed to water (e.g., of gastric fluid), the solvent crosses the polymer coatings and dissolves the active agent, leading to a gradient in solute concentration that drives even more water inside. To accommodate this, the coating must expand, and wall stresses are developed. According to the osmotic driving force, the coating ruptures, and the active is released. Thus, using different coating thicknesses, particles can be programmed to burst at different times.

The original time-release capsules were based on this principle. Moreover, tablets or particles coated with a semipermeable membrane that possesses sparse but well-distributed aqueous pores are other examples of the utilization of the osmosis principle to control the release rate. The membrane pores can be created by excipients blended into the membrane, which dissolve upon exposure to water. The pores constitute spaces through the water flows across the semipermeable parts of the membrane, and displace the dissolved active agent through the aqueous pores into the release medium.[72]

In comparison with drug delivery systems based on diffusion and erosion, osmotic systems tend to be less volume efficient and more complex in design. However, osmotic systems also tend to provide better zero-order delivery and to deliver a greater percentage of the drug loading at a zero-order delivery rate.

Swelling: Many materials display the characteristic of swelling when in contact with water. This is due to their hydrophilic behaviour and the interaction between water and their molecules. Polymers are the main materials employed for preparation of controlled drug release systems, and their polymer chains can organise in a three-dimensional fashion. When a polymer network is surrounded by water, the network expands, and chemical or physical bonds are formed. Compared to osmosis, the swelling process is very similar. Water enters the polymer relatively rapidly, while dissolution of the polymer into water, if it occurs, is comparatively slow because of the need for polymer chains to disentangle.[72] This expansion of volume and the consequent emergence of greater spaces between the polymeric chains can be used to control the release of active agents from polymeric systems (matrix or reservoir).

Targeting: Drug targeting is defined as the ability of the active agent to accumulate in the target site selectively and quantitatively, independent of the site and methods of administration. The local concentration of the drug at the site(s) should be high, while its concentration in other non-target organs and tissues should be below certain minimal levels to prevent negative side effects. Thus, drug targeting is a very important mechanism of drug delivery control. A system with optimal targeting properties should contain structural features that specifically interact with the designated target, for example, a particular receptor utilizing ligand–receptor interactions. Ideally, such a receptor should only be associated with a diseased organ or tissue.

The concept of drug targeting was initially used to describe the possible in vivo action of an anticancer drug conjugated to a monoclonal antibody that is specific to a surface antigen on target cancer cells. However, targeting can occur at the specific organ (e.g., brain to treat Parkinson's, Alzheimer's and Creutzfeldt–Jakob disease or targeting the lung in the treatment of cystic fibrosis), tissue (e.g., targeting site of inflammation or tumours), cellular (e.g., targeting to Trastuzumab to human epidermal growth factor receptor-2 and cancer cells), subcellular compartment or organelle level (e.g., targeting to cytoplasm, proteins, receptors, mitochondria, DNA and gene therapy applications), or invading organisms (e.g., targeting viruses, parasites and bacteria), and a range of targeting systems were developed.

There are different forms of targeting: passive and active.

In passive targeting, the distribution of the system is dictated by local physiological conditions or by the mononuclear phagocyte system. Thus, carrier systems are taken up or trapped in organs such as the lung, liver, and spleen by virtue of their size and their surface properties such as size and charge. This type of targeting can be used to target hepatic cells and spleen macrophages, and this site-specific mechanism of clearance is a feature of the immune system. For example, passive targeting therapeutically can be used for the treatment of lysosomal enzyme deficiencies (e.g., Gaucher's disease, caused by a deficiency of the enzyme glucosylceramidase) or the treatment of macrophage intracellular microbial, viral or bacterial disease (e.g., visceral leishmaniasis).

In active targeting, the active element is the interaction of surface ligands with specific associated receptors to aid affinity with targets. These targeting groups are generally covalent interactions, rather than noncovalent, attached to the active agent or the surface of the carrier. The carrier system should be designed to avoid the passive targeting route, mainly the phagocytes of the mononuclear phagocyte system. There are various molecules/receptors that can be used to perform active targeting: folate receptors over-expressed in tumour tissues, antibody-antigen targeting, lectin-glycoprotein targeting, and physical targeting such as magnetically controlled drug delivery".

3 Materials and methods

3.1 Synthesis of DMSN. Cetyltrimethylammonium chloride (CTAC) solution (25 wt % in H_2O), triethanolamine (TEA), tetraethyl orthosilicate (TEOS), 1,2-dichlorbenzene, ethanol absolute, ammonium nitrate, calcium nitrate tetrahydrate, methanol and ethanol all as reagent grade were purchased from Sigma Aldrich. In a typical synthesis, 6 mL of cetyltrimethylammonium chloride (CTAC) solution (25 wt % in H_2O) and 0.1780 g triethanolamine (TEA) were added to 54 mL Milli-Q water (18.2 MW) and stirred at 70 °C for 1 h in a 100 mL 3-neck round-bottomed flask with a KPG stirrer (155 rpm). The heated water-CTAC-TEA solution was underlaid with 20 mL of tetraethyl orthosilicate (TEOS) in 1,2-dichlorbenzene (20 v/v %) without stirring. The stirrer was adjusted right above the boundary layer in the water phase, and the stirring rate was set to 155 rpm carefully to avoid complex mixing patterns which leads to abrupt diffusion. After the reaction was kept at 70 °C for up to 24h, the organic lower phase was removed and collected by centrifugation (9,000 rpm / 20 min). Particles were kept in ethanol right after synthesis until washing by means of PBS. This is especially important in terms of the particles´ high tendency to agglomerate in a buffer solution. Total duration of consumption for each batch was approximately a year. TEM imaging and DLS measurements were performed together with biological assays each time during the period between 6 months and one year storage to control stability status.

3.2 Synthesis of $DMSN_{OPT}$. In a systematic study, DMSNs synthesised by Kienzle, Kurch and co-workers published method were optimised and adapted. The resulting products from synthesis were collected by centrifugation (9,000 rpm / 20 min) and washed several times with ethanol to remove residual reactants. Then for template extraction, DMSN (in ethanol) were extracted 3 times with 1 wt % ammonium nitrate at 80 °C for 1 h/ 310 rpm to remove the surfactant template. The washed DMSN (200 mg wet) was mixed with 40 mL of a calcium nitrate tetrahydrate solution (0.1 M dissolved into methanol) and then stirred with KPG stirrer (220 rpm) at 50 °C for 48 h. The final particles were washed with ethanol several times and kept in fridge (2-7 °C).

3.3 Synthesis of DMSN with Fe_3O_4 core shell system.

Synthesis of iron oxide nanoparticles and surface defunctionalisation. FeOOH brownish/red powder, 1-octadecene, oleic acid, acetone, cyclohexane, isopropanol, tetramethylammoniumhydroxide (25 wt% in water) and tetrahydrofuran all as reagent grade were purchased from Sigma Aldrich. In a 100 mL 3-neck round bottom flask 358 mg of the FeOOH precursor were mixed with 10.02 g of octadecene and 4.47 g of oleic acid. The mixture was ultrasonicated for 5 min. Afterwards, the mixture was degassed under vacuum (Schlenk: $5 \cdot 10^{-2}$ mbar) at 500 rpm for 15 min. After switching towards Argon the stirring speed was reduced to 300 rpm. The reaction and nanoparticle formation was achieved by heating the solution within around one hour from room temperature to 320 °C with a heating mantle under Argon atmosphere.

The resulting dark nanoparticle dispersion was divided into 4 centrifuge tubes (V=50 mL) each with a volume of 7.5 mL. The precipitation was induced by adding acetone up to 45 mL, mixing and resting for 1 h. After equilibration the precipitate was gathered by centrifuging the dispersion for 10 min at 9000 rpm. Each centrifuge tube was filled with 5 mL cyclohexane and the precipitates were redispersed via ultrasound. The precipitation was induced by adding up to 45 mL of isopropanol. The precipitates were merged into one centrifuge tube in 7.5 mL cyclohexane (total volume amount) and the precipitation was induced by adding up to 45 mL with isopropanol. After this, the precipitate was washed again 4 times by adding 5 mL of cyclohexane and precipitating with isopropanol (up to 45 mL). The precipitate was gathered in 4-5 mL of cyclohexane in a brown glass vial for further use.

For defunctionalisation of the particles, 1 mL of the iron oxide nanoparticle suspension was mixed with 4 mL of cyclohexane. To this solution, a solution of 1mL tetramethylammonium hydroxide (25 wt% in water) with 4 mL of Milli-Q water was added to yield a biphasic mixture. To this mixture 2 mL of isopropanol were added for mixing the phase borders. The mixture was mixed (strong around 1000 rpm) for 4 h. After transferring the mixture into a centrifuge tube the precipitation was induced by adding tetrahydrofurane. The precipitate was gathered by centrifugation at 9000 rpm. The residue was washed two times by dispersing the particles in water and precipitation via addition of tetrahydrofuran. The residue was shortly dried under a slight nitrogen flow and then dispersed in a mixture of 1:1 ethanol:water. The resulting

dispersion was centrifuged for 1 min at 2500 rpm to remove agglomerates. The supernatant was collected and kept in a glass vial for further use (8.7 mg/mL nanoparticle solution).

Encapsulation of iron oxide in DMSN. 10.22 g of a Fe_3O_4 seed particle solution were added slowly into the water phase of the biphasic stratification reaction prior to TEOS addition. Heterogeneous nucleation leads to the encapsulation of the iron oxide core into a silica shell.

3.4 TEM imaging and staining: High contrast and resolution TEM images were acquired with a FEI Tecnai^{TM} G^2 Spirit (120 kV voltage, Oregon, USA) instrument equipped with an on axis Gatan US1000 2kx2k CCD camera system. Image post-processing was performed in imageJ. The protocol used for the deep-stain-embedded image shown in this work was adopted from method described in Indiana university electron microscopy centre website.

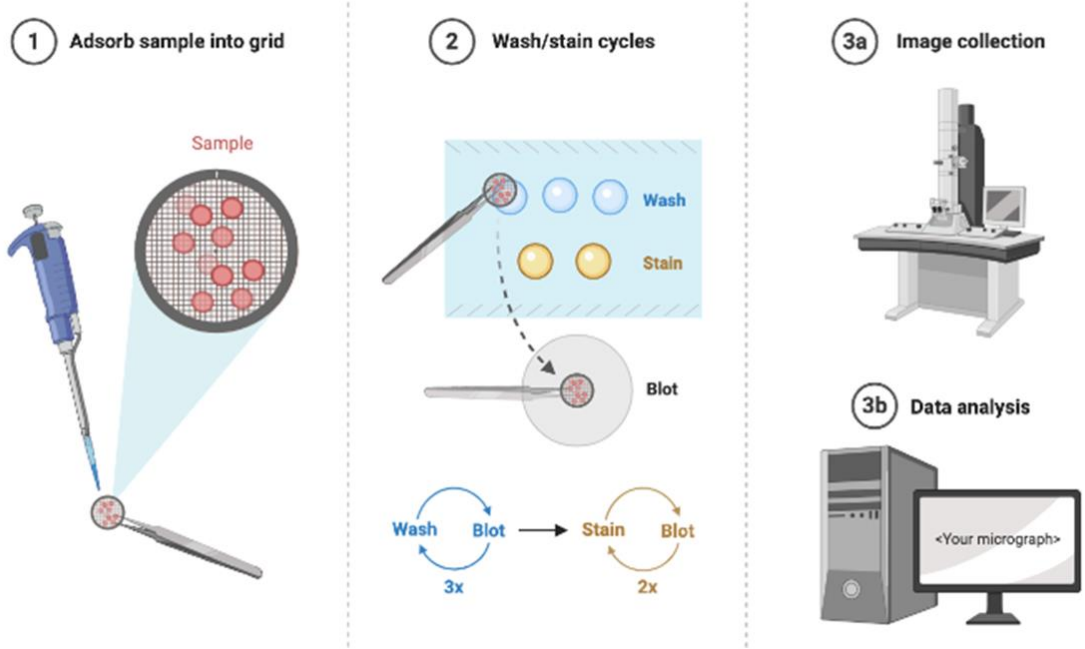

Figure 5. Deep-stain-embedded image procedure. (1) 3 µL of sample was applied to the grid (CF300-CU). Kept in air 25 sec. (2) blotting/washing and then immediately placing the grid in stain repeatedly. Stain solution: 1 mL of distilled water + 0.16 g of ammonium molybdate (16% (w/v)). The pH was adjusted to 7.0 using 10 N NaOH. The solution was passed through a 0.2 micron filter. (3) Waving the grid in air to dry and then immediately using for TEM. With permission from biorender.com

3.5 Surface area and pore size analysis. $DMSN_{OPT}$ desiccated powder were transferred into a measuring cell. Before testing, all possible previously physisorbed species were outgassed under high vacuum. Sorption measurements were performed at 77.2 K using liquid nitrogen. Total pore volume was calculated using the gas amount adsorbed at a maximum relative pressure (P/P_0) of 0.990. Pore size of samples from adsorption branches of isotherms were calculated using the Barrett-Joyner-Halenda (BJH) formula. Specific surface area was calculated using the Brunauer-Emmett-Teller (BET) formula (3P Instruments Micro 300, Germany).

3.6 NMR measurement and CTAC contamination. Experiments were performed on a Bruker ARX 400 spectrometer using a ^{1}H frequency of 399.83 MHz and a ^{13}C frequency of 100.54 MHz. Particles (8 mg) were dissolved in 540 µL of D_2O+60 µL NaOD, obtained data analysed using Mnova NMR software and percentages calculated.

3.7 ATR-FTIR Spectroscopy. The attenuated total reflection (ATR) FTIR spectra were recorded on a Nicolet iS10 spectrometer (Thermo scientific) using a frequency range from 0 to 5000 cm^{-1}.

3.8 Zetasizer surface charge and dynamic light scattering (DLS). Hydrodynamic particle size and net surface charge in terms of zeta-potential of DMSN were determined at 20 °C by DLS (Malvern Zetasizer Nano ZS).

3.9 Testing TNF-α sensitivity of mouse fibrosarcoma with MTT assay. TNF-α cell sensitivity to indicator WeHi cell line after 24 hours was investigated. The range of TNF-α concentration was between 1 µg/mL to 1 fg/mL and the serial dilutions ratio x) 1:2 within the plate and y) 1:10 in small tubes (vortexing between each transfer). Different dilutions of TNF-α (50 µL/well) were plated in a 96 well plate in triplicate. WeHi cells ($2{,}5x10^4$ cells per well- 50 µL/well) were incubated with TNF-α for 24 hours. Untreated cells served as positive (live) control and cells treated with 10% DMSO served as negative (dead) control. After ~ 24 hours, 10 µL/well MTT solution (5 mg/mL stock) was added, and the cells were kept in incubator for 4 hours (purple colour develops within this time for the aforementioned cell density). Wells were also checked under microscope to observe the formation of formazan crystals. As the last step of the procedure, 100 µL of detergent reagent (isopropanol with Triton-X 100 (10%) and 2 drops of 0.1 M HCl) was added to each well and pipetted up and down to dissolve the crystals for measurement (this was also controlled under a microscope). Then the whole plate was sealed and kept at air conditioning room overnight in the dark. On the

next day, the contents of the plate were transferred to a new plate for reducing measurement background.

3.10 TNF-α release profile of DMSN$_{OPT}$, collecting supernatants and ELISA. Loading and release profile of nanoparticles were tested via ELISA (dilution in the range of 0 to 10000). For DMSN loading, TNF-α Beromun (Boehringer Ingelheim, Germany) and DMSN were mixed at different ratios and kept under constant shaking 700 rpm/ 24 h at 4 °C. After TNF-α loading, release at different time points was measured by way of centrifuging at 15000 rpm/ 15 min, collecting supernatants and performing ELISA (according to BD OptEIA™ human TNF alpha ELISA and reagent set). Absorbance was read at 450 nm via Absorbance microplate reader BioTek™ELX808™, Ratingen.

3.11 Coating of TNF-α loaded DMSN$_{OPT}$ with P-L-L (or sarcosine-lysine). For coating, at first particles (300 µg) were washed 2 times with PBS (DPBS). After encapsulation step, Sigma Poly-L-lysine–FITC Labeled (or Sarcosine-Lysine synthesised by [redacted] was added to the loaded-nanoparticle dispersion at a ratio of 1:1-1:3-1:6 and kept shaking at 700 rpm/ 4 °C for another 24 h. To remove free TNF-a and wash extra polymer, samples were centrifuged at 15000 rpm, supernatant discarded and coated loaded-DMSN re-suspended in fresh PBS using sonication, twice.

3.12 Assessing nanoparticle toxicity. First, the highest concentrations (no aggregation) of the particles in medium (DMEM+10% FCS) were made. To execute this, stable particles, which were stored in ethanol for less than three months, were washed with PBS twice, and then medium was added. Particles were plated via serial dilutions within the plate (24 well-500 µL volume each well). Then WeHi cells ($1x10^5$ per well cell density) were incubated with different amounts of both uncoated and coated particles for 24 hours. As live control WeHi cells were cultured in DMEM+10% FCS without particles and for dead control with 10% DMSO**.**

3.13 Culture medium, cytokines and antibodies. For feeding and maturation experiments, RPMI 1640 media (gibco), X-VIVO^{TM} 15 serum-free hematopoietic cell medium (Lonza), EDTA disodium salt 2-hydrate (AppliChem), Pen Strep (gibco), human serum albumin 20% (HSA, CSL Behring), LEUKINE® sargramostim (Sanofi, 800 U/mL), rh IL-4 (ImmunoTools, 100U/mL), TNF-α (10ng/mL), PGE_2 (Cayman, 1µg/mL), FITC conjugated goat anti-mouse IgG & PE conjugated donkey anti-mouse

IgG (αrF and αmPE - Jackson ImmunoResearch, 5µg/mL), CD80/CD83 (Beckman Coulter, 250µg/mL) and CD86 (AbD Serotec, 1mg/mL) were used.

3.14 Isolation of PBMCs from buffy coat & generation of immature monocyte-derived dendritic cells. At first, 15 mL of Bicoll (BIO&SELL, density 1,077 g/mL) was pipetted into conical tubes (50 mL). The Bicoll in tubes were overlayed with equal amount of buffy coat (using sterile scissor and 10 mL glass pipette tilted to create no flow). These tubes were centrifuged at 800 G, for 30 min at 24˚C in a swinging bucket rotor without brake. The upper layer (plasma) was removed to another tube and heated directly for 1 hour at 56˚C (to inactivate proteins). Then it was centrifuged twice at 1000 G for 15 min at 4˚C (to precipitate degraded proteins). The undisturbed mononuclear cell layer at the interphase (lymphocytes and monocytes) was carefully transferred to a new 50 mL conical tube and filled up with wash buffer (1 mL EDTA, 0.5 M in 500 mL of cold PBS). Then mixed and centrifuged at 350 G for 6 min at 4˚C. This step was repeated as many times as the supernatant became transparent. At this stage, cell pellet was re-suspended and cells were counted (Trypan blue solution, Sigma). Each buffy coat contained PBMCs in the range from 180 to 380 million cells depending on the donor.

After preparing fresh PBMCs as described above, 10-15*10^6 PBMCs per well were plated into a 6-wells plate with 2 mL of RPMI (plus 1-2% heat inactivated plasma as nutrient) per well as medium. The plate was incubated (37 °C/5% CO_2 humidified incubator HERAcell 240i, Thermo Fisher Scientific) for up to an hour (the adherence is visible under microscope). After that, medium containing non-adherent cells (lymphocytes) was discarded (followed by washing the plate with PBS twice). Then, culture medium (X-VIVO 15 + GM-CSF/IL-4/1%plasma) was added to the cells in 3 mL per well and the plate was placed in incubator. Cells were fed with culture medium in 1 mL per well (1 mL of each well was removed and 1 mL fresh media was added) after 2 and 4 days (or 3 and 5, in case the maturation is at day 6). After 5-6 days, the loosely adherent or non-adherent cells should display typical dendritic cell morphology and surface markers (CD86, HLA-DR). The monocytes count in each plate were within the range of 2 to 6 million depending on the donor.

3.15 Light microscopy of human DCs. A Carl Zeiss Axiovert 135 microscope was used for imaging and a Leica Microsystems SM-LUX for cell counting.

3.16 Flow cytometry. Cells (mature and immature) were first washed in the 6-wells plate and transferred into 15 mL vials. Then they were washed once with FACS buffer

(500 mL DPBS+12.5 mL HSA+1 mL EDTA+500 µL sandaglobin) and resuspended again in flow cytometry cell number range (10^5 to 10^6 cells). Depending on the setup of each experiment, 20 µL of the primary antibodies (HLA-DR,CD80,CD83,CD86) were added to the relevant wells containing cells (plus controls). The 96-well plate was placed in the fridge for 20 min. Afterwards, cells were washed again with 100 µL FACS buffer. At this stage, 20 µL of the secondary antibodies (αmPE and αrF) were combined with the rest and incubated in a refrigerator for 20 min. Right before the readout, the washing step with FACS buffer was repeated (Flow Cytometry BD FACSVia™, BD Biosciences, Heidelberg)

3.17 Preparation of T cell. (According to CD4+ isolation kit, Miltenyi Biotec)

3.18 Allogenic MLR. Naive CD4+ T cells isolated from cord blood were stimulated with allogenic DCs. Cells were cultured in flat-bottom 96-well plates in a final volume of 200mL/well X-VIVO-15 and in different ratios (1:10-1:640 DC:TC) for 4 d and an additional 16 h thymidine methyl-^{3}H (PerkinElmer) pulse. Thymidine incorporation was measured using a scintillation counter 1205 Betaplate® (LKB, Schweden).

4 Results and discussion

4.1 Synthesis, optimisation and characterisation of the $DMSN_{OPT}$

$DMSN_{OPT}$ was prepared by a sol-gel bi-phase reaction which takes place at the interface of precursor (TEOS) and surfactant (CTAC) solutions. The synthesis is generally carried out in an organic cosolvent through simultaneous or sequential reactions of hydrolysis and polycondensation, releasing water and/or alcohol.[73] It is a possible advantage to add other reactants (like catalysts, nanoparticles as core or fluorescent dyes) based on needed structure and characteristics as long as the interface remains undisturbed, and the pore size can also be controlled by various routes.[59] On the following pages, it is shown how to create core-shell particles with respect to the basic procedure.

In the past, Shin and co-workers enlarged MSN pores with divalent calcium and magnesium salts and extracted template simultaneously. Although, they have reported substantial decreases in BET surface areas and total pore volumes.[74] The current study aimed to prevent losing surface area. CTAC was successfully extracted with ammonium nitrate, followed by the reaction with calcium nitrate tetrahydrate solution dissolved into methanol. These combined reactions mostly lead to ion exchange/corrosion of the silica interior walls (Figure 6). A number of modifications have been made to the speed and time of stirring along with the number of steps to maintain high BET surface area and increase pore diameter at the same time. In the table 2, we can see that the objective was met. Additionally, the total pore volume did not decrease, but quite the opposite. It is debatable whether utilizing these salts and repetition has increased particle stability.

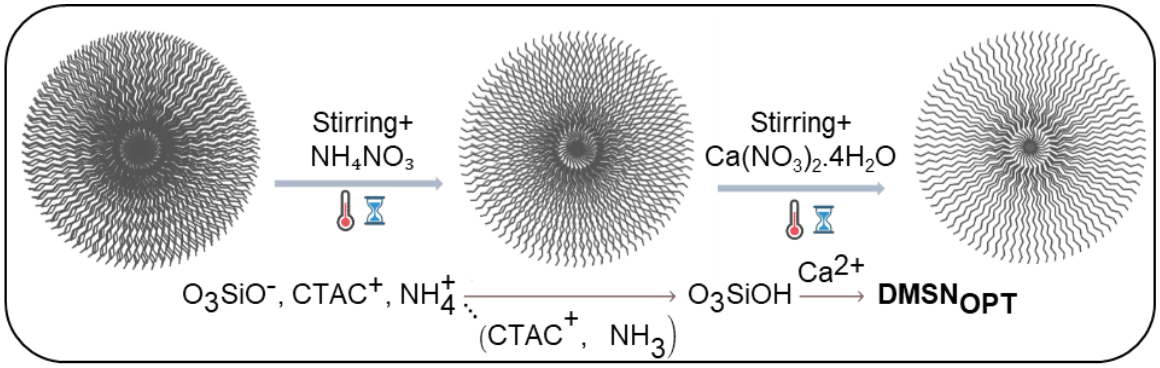

Figure 6. **Schematic overview of $DMSN_{OPT}$ synthesis.** To increase pore size, DMSN (in ethanol) were extracted three times with 1 wt % ammonium nitrate at 80 °C for 1 h/ 310 rpm to remove the surfactant template. The washed particles were mixed with calcium nitrate tetrahydrate solution (0.1 M dissolved into methanol) and then stirred at 50 °C for 48 h/ 220 rpm. The final particles were washed with ethanol several times.

As result, particle diameters in the range of 100-160 nm are produced (Figure 7). i.e., the particle size is slightly affected by the process. The range of particle sizes has shifted downward from average 160 nm to 130 nm.[52] FTIR measurement (Figure 8) of dried particles powder shows asymmetric and symmetric vibrations of Si-O at around 1090 cm^{-1} and 795 cm^{-1} attributed to polycondensation plus the weaker asymmetric vibration of Si-OH at around 950 cm^{-1} for hydrolysis reaction.[75] Figure 9 shows selected area electron diffraction (SAED) pattern of $DMSN_{OPT}$. The same applies for DMSN; under the given reaction conditions of temperature and pressure, amorphous silica is formed.

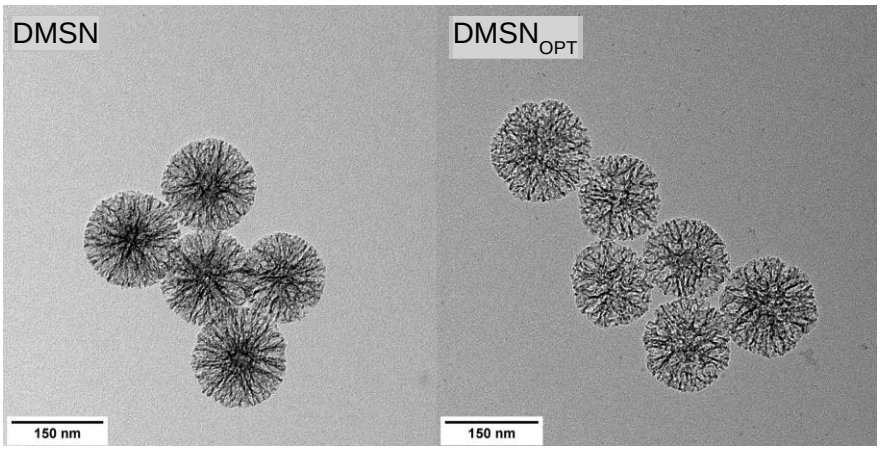

Figure 7. **One representative TEM image of the $DMSN_{OPT}$**. Particle diameter ranged between 100 nm and 160 nm wih an average of 130 nm (imageJ).

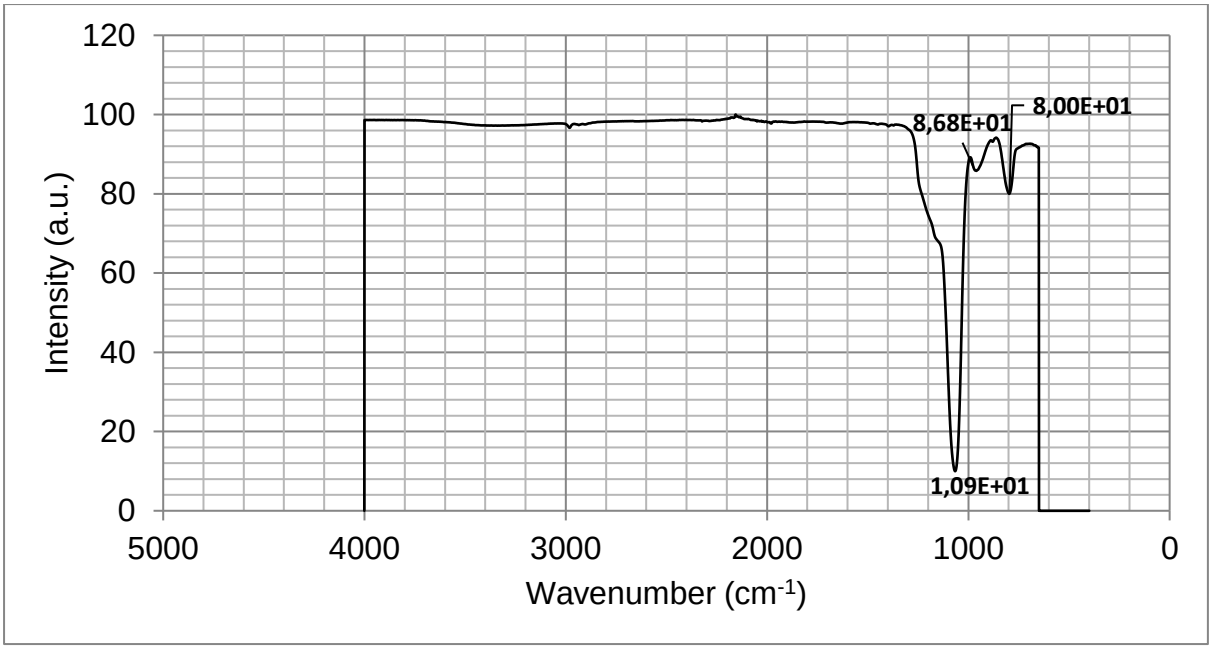

Figure 8. IR spectra of overnight exsiccated DMSN$_{OPT}$ powder.

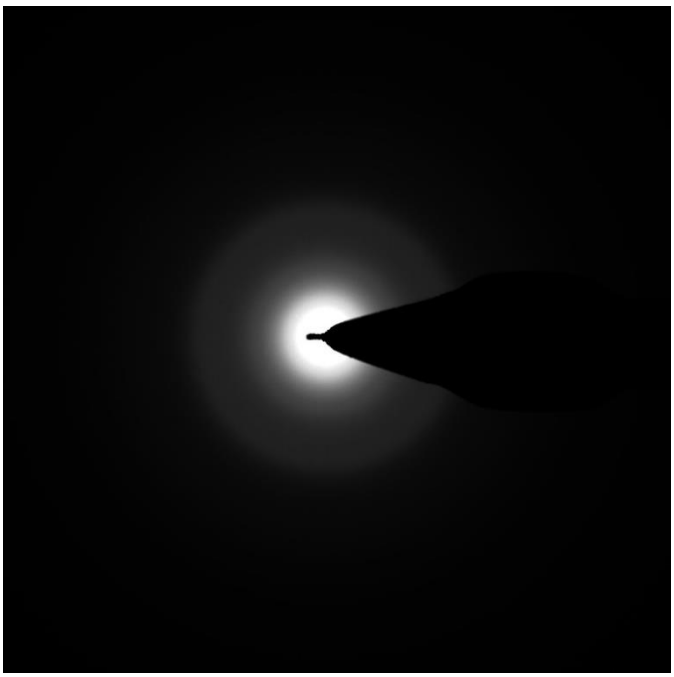

Figure 9. Selected area electron diffraction pattern of DMSN$_{OPT}$.

Three different batches of DMSN$_{OPT}$ were prepared according to the procedure described in the materials and methods. N_2 gas physisorption results are represented in Table 1. DMSN$_{OPT}$ undergoes physisorption in three distinct phases: monolayer and multilayer adsorption and pore condensation. In multilayer adsorption not all molecules are in direct contact with the adsorbent surface. Then, the gas is condensed into a

liquid-like phase in every pore. Adsorption hysteresis arises when the adsorption and desorption curves do not coincide as is the case in Figure 11.[76] Porosity is defined as the ratio of the total pore volume to the volume of the particle or agglomerate (sum of solid and pore volumes). Therefore, we can plug the values into the equation: (density of silica nanoparticles ~2 g/cm^3)

$$Pt(avg.) = \frac{Vp}{Vt} = \frac{2.06}{2.06+0.5} * 100 = 80.5\%$$

In each repetition of this (Figure 6) reaction, a proportion of the primary pores becomes bigger pores as a result of surfactant extraction and/or collapse of the interior network. The findings of the batch variation in Table 1 suggest that the final pore features can be controlled relatively well. The results have shown that the synthesis procedures allow the preparation of reproducible batches with optimal parameters (BET surface area over 500 m^2/g, total pore volume 2.07±0.47cm^3/g and later, very high over 95% encapsulation efficiency of TNF-α) and the synthesis procedures could be modified for scale up preparation of DMSN$_{OPT}$.

Table 1. Characteristics of DMSN$_{OPT}$ for three independent batches. Shown is the BET surface area, total pore volume, average pore diameter peak 1 and 2. Total pore Volume was measured at p/p$_0$= 0.990.

Batch	BET surface area (m²/g)	Total pore volume (cm³/g)	Most frequent pore diameter in peak 1 (nm)	Most frequent pore diameter in peak 2 (nm)
#1	521	2.6	14.7	40.0
#2	513	1.7	7.9	51.0
#3	508	1.9	9.4	54.6

It is shown in the representative graph of one batch (Figure 10) that DMSN$_{OPT}$ has a bi-model pore size distribution; mesopores and hollow structure (upper limit 100 nm) in comparison to DMSN with only mesopores prepared by Kienzle et al.[52] Core-cone structured monodisperse mesoporous silica nanoparticles with ultra-large cavities for protein delivery have been prepared[53] using the same bi-phase reaction. Their loading capacity has increased, so we will discuss it later in encapsulation section. Only one

peak can be seen in their pore size distribution curve at 45 nm. These findings suggest that the encapsulation efficiency is directly related to the presented modification.

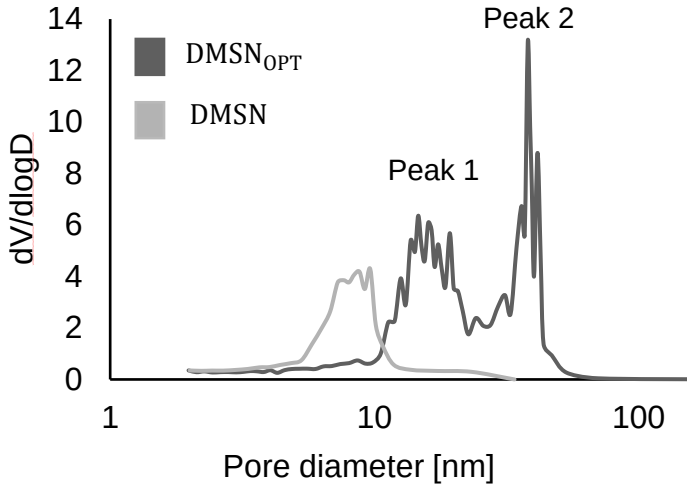

Figure 10. One representative desorption pore size distribution plot for DMSN vs DMSN$_{OPT}$ measured by BJH (n=3).

In light of the hysteresis loops (Figure 11), DMSN$_{OPT}$ shows a more gradual curve and less distinctive point B which indicates a significant amount of overlap of monolayer coverage and the onset of multilayer adsorption.[76] These particles include a narrow range of uniform mesopores (H1 loop). The steep, narrow loop is a sign of delayed condensation on the adsorption branch. Meanwhile, the type H2(b) loop is associated with pore blocking (delayed desorption) first and foremost due to the size of the pores. DMSN$_{OPT}$ has about twice the average pore diameter of DMSN. However, the porosity is not doubled (69 to 80%). This further on implies the pore diameter is a more important factor for the cargo. Table 2 summarises the characteristics of both nanoparticles.

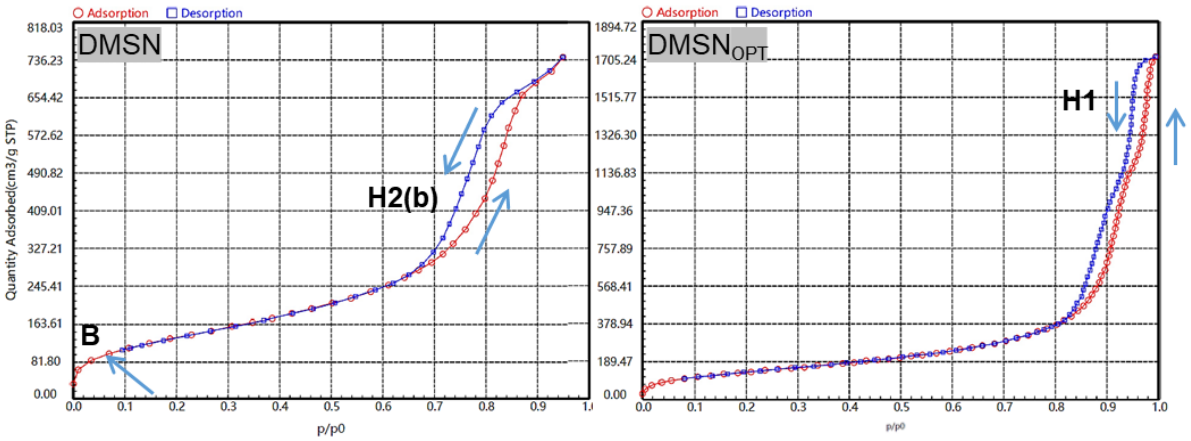

Figure 11. Hysteresis loops for DMSN vs $DMSN_{OPT}$ measured by BET (n=3).

Table 2. Characteristics of DMSN and $DMSN_{OPT}$. Shown is the BET surface area, total pore volume, average pore diameter.

Sample	BET surface area (m^2/g)	Total pore volume (cm^3/g)	Average pore diameter (nm)
DMSN	504	1.1	9.1
$DMSN_{OPT}$	521	2.6	20.2

The influence of "washing steps" was not only in the context of the control of pore size, but also the removal of the toxic CTAC, which is very relevant for the further development of the $DMSN_{OPT}$ for the delivery of TNF-α. The results (Figure 12, left) have shown that three washing steps will be sufficient to remove almost completely (4%) the CTAC from $DMSN_{OPT}$. In spite of the fact that silica is generally regarded as a non-toxic compound, the toxicity of nano-scaled investigated $DMSN_{OPT}$ needs to be re-evaluated, since parameters like size, surface properties, shape and structure can affect it.[77] Thus, contamination examination is accompanied by cell viability assay which shows no toxicity for concentrations below 25 µg/mL (Figure 12, right) as well as no detectable endotoxin (<0.050 EU/mL).

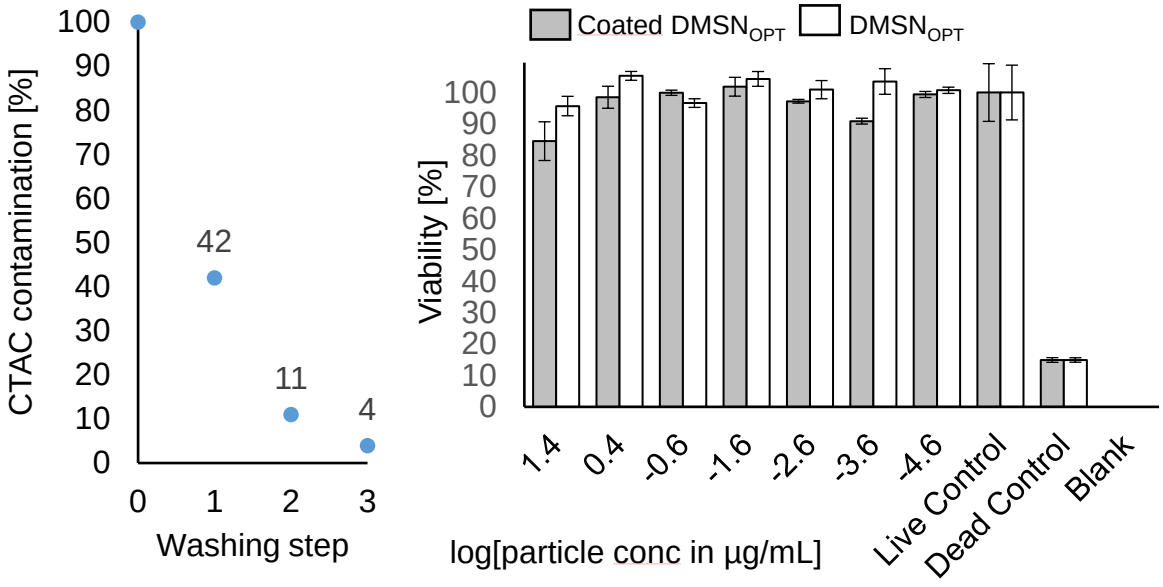

Figure 12. Toxicity and purity of coated and uncoated DMSN$_{OPT}$. Shown left is removal of CTAC polymer from DMSN$_{OPT}$ after repetitive washing steps (0-3) measured via ^{1}H NMR and calculated via Mnova. Right: after 24 h of treatment with uncoated and coated DMSN$_{OPT}$ at various concentrations, cell viability was measured using MTT. No toxicity for concentrations below 25 µg/mL was observed (n=3).

Lastly, DLS and zetasizer measurements were performed for DMSN$_{OPT}$. The diagram in Figure 13 is the primary result and shows the intensity of scattered light from each size population present in the sample. The average hydrodynamic particle size in ethanol and PBS is in the range of 194 and 208 nm, which shows particle size stability. In addition, the zeta potential of the DMSN$_{OPT}$ in the investigated media were in the narrow range of -9.26 to -8.19 mV (n=3).

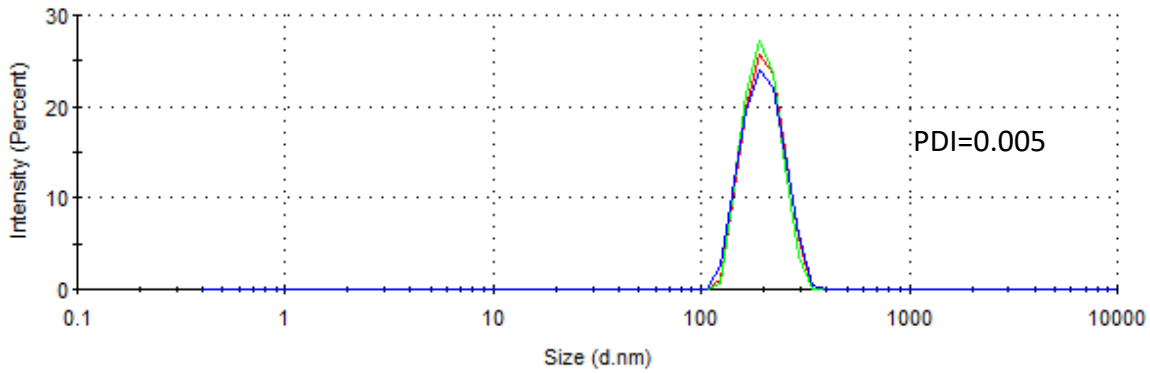

Figure 13. Particle size distribution curve of $DMSN_{OPT}$ stored in ethanol for 4 months.

4.2 Synthesis and characterisation of the Fe_3O_4 core shell DMSN (magnetic)

Since the integration of mesoporous silica with magnetic particles is of great interest for practical applications, mesoporous DMSN with magnetic core was synthesised. The goal is to minimise the obstacles associated with the synthesis of these particles such as low Fe_3O_4 mass fraction, abnormal structures and low dispersity in water.[78] Magnetic particles with a strong magnetic response and high encapsulation and dispersibility are the only particles that may be competent with $DMSN_{OPT}$ in the current study. Homogeneously distributed iron oxide nanoparticles (synthesised following ref. [79] and shown in Figure 14, C) were encapsulated in the silica shell through the same reaction solution as before. The core was freshly prepared each time (very important, since these metal oxide nanoparticles intend to form stable agglomerates rapidly). To reduce the formation of free silica nanoparticles, the ratio of silica precursor to Fe_3O_4 seeds must be adjusted. Magnetic separation of the nanoparticle from free silica was possible by a MS column purchased from Miltenyi Biotec. TEM images of core-shell particles (Figure 14, D) and EDX mapping analysis of O, Si, Fe and Cu (grid) shows a successful incorporation. Figures 14, A) displays element Si of particle shell line scan, while B) shows element Fe peak for the core. Figure 14, E shows that multiple nanoparticles were incorporated into the mesoporous shell as a result of the small size of the Fe_3O_4 seeds.

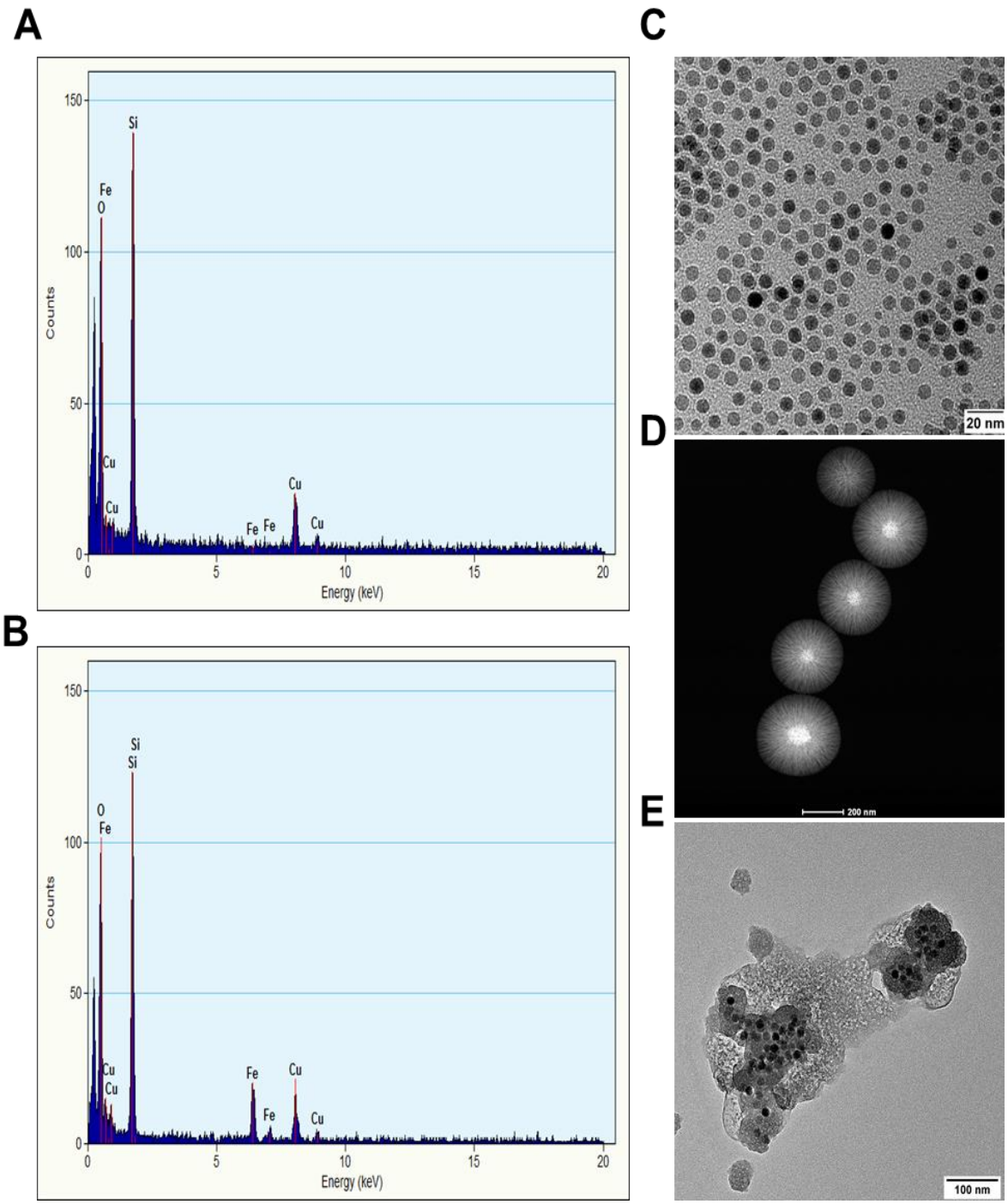

Figure 14. Characterisation of the Fe_3O_4 core shell DMSN (magnetic). A+B) Spectrums of shell and core, respectively. C) Homogeneously distributed iron oxide nanoparticles. The average size is 5 nm (imageJ). D) Fe_3O_4 core shell DMSN. E) Biodegradation of the magnetic nanoparticles in DMEM + 10% FCS at 37 °C after 18 h.

As an attempt to control and verify the reproducibility of the procedure, the synthesis was repeated under the same conditions. A comparative dataset of the pore structure characteristics has been gathered in Table 3. Fe_3O_4 core shell DMSN, has overall a

higher number of smaller pores (compared to $DMSN_{OPT}$). These particles are about three times bigger than $DMSN_{OPT}$ in diameter, but BET surface area is almost in the same range.

Table 3. Characteristics of magnetic DMSN for three independent batches. Shown is the BET surface area, total pore volume, average pore diameter, average particle diameter. Total pore Volume was measured at p/p_0= 0.990.

Batch	BET surface area (m^2/g)	Total pore volume (cm^3/g)	Average pore diameter(nm)	Average particle diameter(nm)
#1	556	1.1	8.0	300
#2	523	0.9	6.7	385
#3	558	1.3	9.1	285

The toxicity of non-coated and unloaded magnetic particles was assessed in different concentrations ranging from 200 µg/mL to 1.6 µg/mL utilizing flow cytometry. The gating method with 7-AAD as a proficient marker is used to select and categorise cells of interest which are dead cells in this experiment.[80] 7-AAD is a fluorescent DNA binding dye that is membrane impermeant and therefore generally excluded from live cells and early apoptotic cells, but stains necrotic and late apoptotic cells with compromised membrane integrity. SSC versus 7-aad plot is shown in Figure 15. In each graph, there is a dead cell region consisting of a certain number of points (in percentage). Particles show a high toxic effect at 200 µg/mL particle concentration (~ 80%). In the range of 25-100 µg/mL they only show a slight toxic effect (toxicity ~ 5-15%). For in vitro experiments, particle concentration around 25 µg/mL (highest) is recommended.

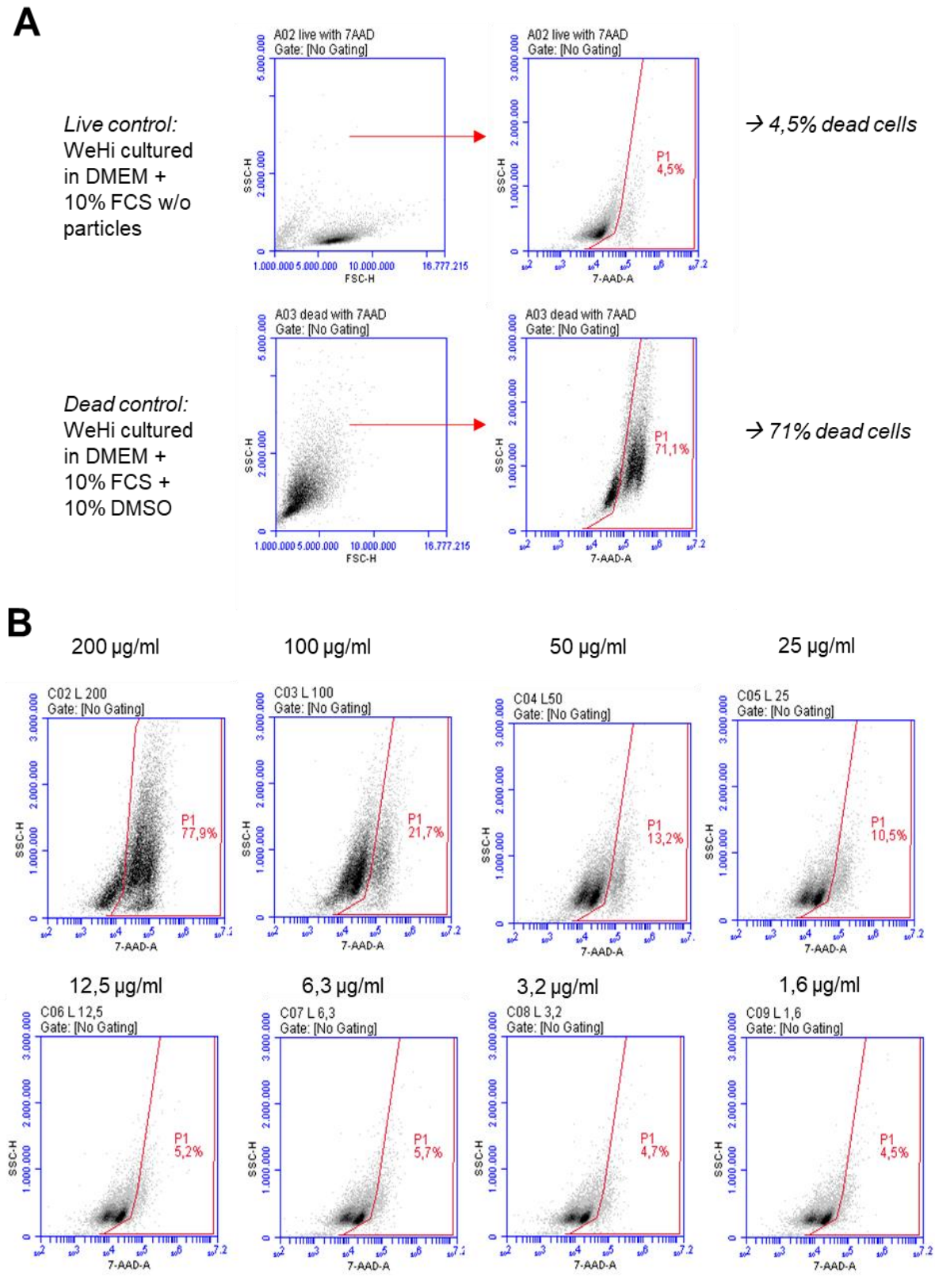

Figure 15. Toxicity of magnetic DMSN. A) Live and dead controls specifications. B) Toxicity results in concentrations ranging from 200 µg/mL to 1.6 µg/mL.

4.3 Biological activity of TNF-α

To validate all further experiments with TNF-α Beromun as the targeted drug, cell sensitivity to the highly sensitive indicator WeHi cell line after 24 hours was investigated. A clear titration of TNF-α is a sign for its sensitivity. A protein's activity is applied to the function that it serves, which is immune activity in the current study. The concentration of TNF-α used in immune tests is 10 ng/mL. As shown in graph figure 16, the corresponding viability of indicator cells has been stressed (green bar). At 1 pg/mL no toxic effect is observed.

Supernatants of all the investigated TNF-α concentrations (Figure 16) after encapsulation and total release from particles (Figure 19 shows the recovery, *vide infra*) were also tested, and the same level of biological activity was observed, which indicates that the integrity of TNF-α was maintained even after encapsulation.

As a positive note, there is almost no background in this measurement as the negative control is fairly zero. This was only achieved after changing culture medium to DMEM without phenol red + 10% FCS. Additionally, high protein concentrations interfere with the detection of MTT-tetrazolium, and such samples must be diluted prior to assaying.[81] Another proof of correctness is the possible proliferation of the cells at the very low concentration which led to a higher than the normal range viability. The side microscopic images show cell morphology in controls (Figure 16B+C) and highest TNF-α concentration (Figure 16A). Live cells are brighter and refractile, while dead cells usually round up and become detached.

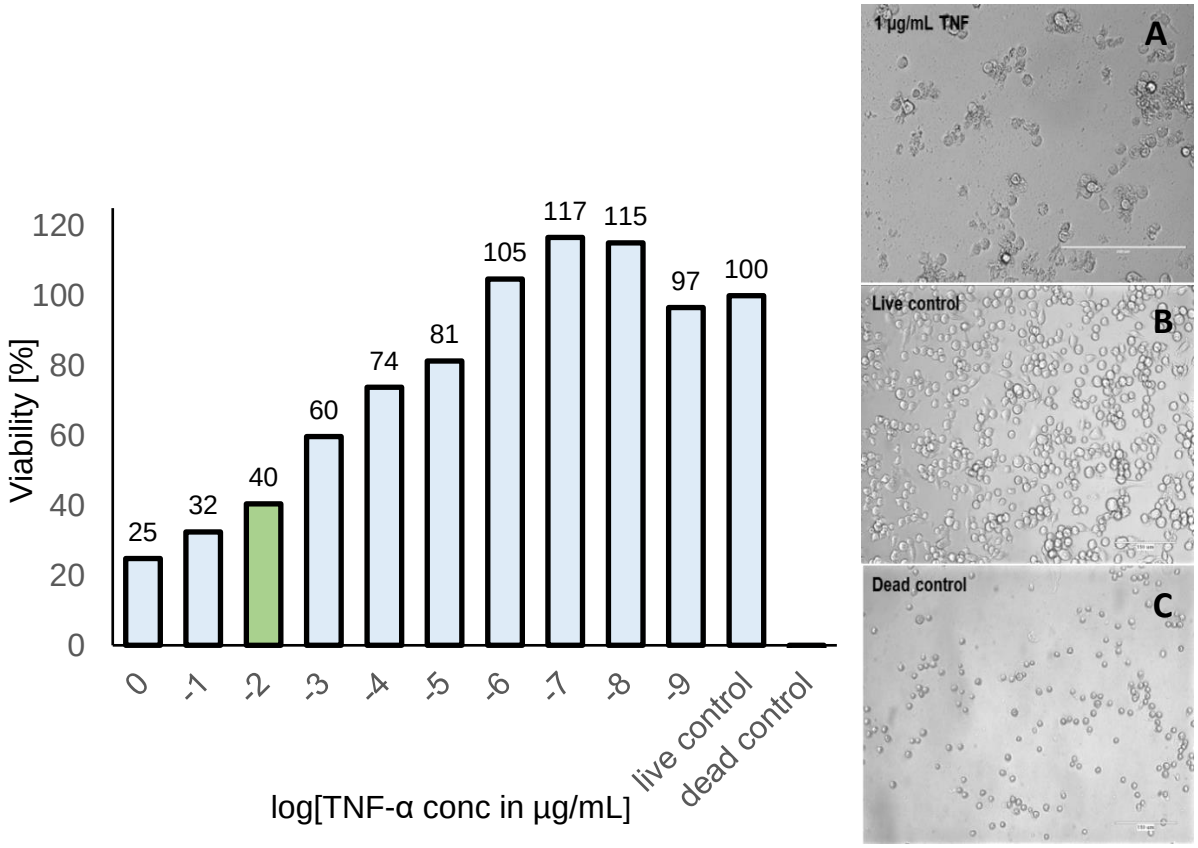

Figure 16. Proof of TNF-α sensitivity/biological activity.

4.4 TNF-α encapsulation

Considering TNF-α encapsulation as a fundamental aspect of this study, the loading of uncoated small pore DMSN and large pore $DMSN_{OPT}$ have been investigated and compared via sandwich ELISA. In a micro-well plate, first antigenic available site of TNF-α in supernatants binds to capture antibody which has been incubated and attached to the surface of the plate overnight (2-7 °C). Using blocking buffer, the plate was prevented from directly contacting the detection antibody and antigen at the same time. The second site binds to the detection antibody. Now here is the tricky part; the secondary detection antibody must recognise a different epitope on the primary one than the capture antibody. In such manner, the amount of TNF-α between two layers of antibodies can be measured through enzymatic detection.[82] The advantage of sandwich ELISA is that the sample (in this case supernatant) does not have to be purified before analysis, and the assay is still very sensitive. The signal of each currently unidentified sample must be compared against those of a standard curve and the concentration of the standard used should span the detection range.

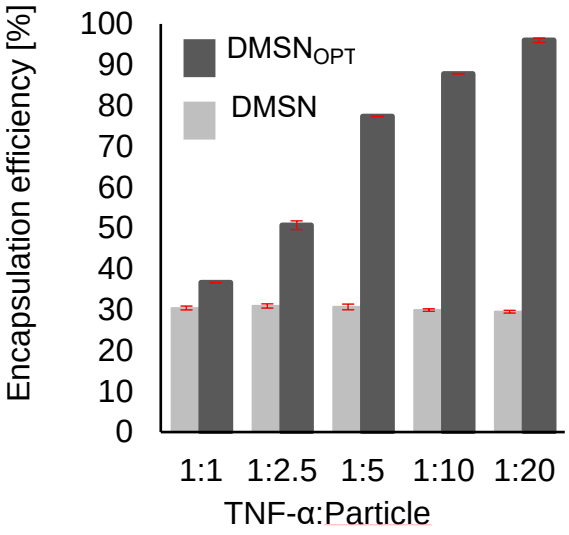

Figure 17. **Comparative analysis of DMSN and DMSN$_{OPT}$ regarding encapsulation efficiency and its dose-dependency.** Bars show mean encapsulation efficiency for each TNF-α to particle ratio. Each represented ELISA has been performed in duplicate.

Published DMSNs [52] were synthesised and tested via ELISA with regard to encapsulation efficiency and compared to the synthesised DMSN$_{OPT}$. The following formula was used to calculate the encapsulation efficiency:

$$encapsulation\ efficiency\ (EE\%) = \frac{total\ drug\ added - free\ nonentrapped\ drug}{total\ drug\ added} * 100$$

The loading capacity of all samples prepared using DMSN reached their maximum of approximately 30% after incubation (Figure 17). It may also show that the amount of adsorbed TNF-α on DMSN outer layer is negligible, otherwise we should have seen a significant increase in TNF-α loading as a result of the increase of TNF-α:DMSN.

The results obtained for the encapsulation efficiency of the DMSNs are relevant limitations to their use for the encapsulation and application of TNF-α and its delivery for clinical application. Therefore, the focus of this research work was the development, optimization, and preparation of the DMSN$_{OPT}$ system, as described here. They have shown great efficiency compared to the previous DMSN as shown above.

Here it has been shown that utilization of the large mesoporous structure can increase the loading of TNF-α up to 96%. Moreover, this study may imply that the encapsulation efficiency is directly controlled by the process of preparing nanoparticles along with the effect of the ratio used for encapsulation. In contrast, Lokras' team showed that the encapsulation efficiency was almost constant (64–78%) throughout the design space, which is an indication that the encapsulation efficiency depends more on the preparation process of the LPNs than on independent variables.[83]

This improvement allows us to minimise the amount of drug used and helps carrying more drug. For the upcoming studies, among different TNF-α : nanoparticle ratios of 1:20 were chosen which showed the highest encapsulation efficiency among all. Because a minor loss of TNF-α during the coating process and the washing steps is inevitable, the goal is to have the highest encapsulation efficiency.

When compared to the work of the Queensland group, a 3-fold difference in encapsulation efficiency was detected, while they observed 1.5-fold.[53] Given that TNF-α is also negatively charged, once again the pore size appears to have a stronger influence than electrostatic interactions (repulsion) between negatively charged particles and TNF-α.

4.5 TNF-α release

After encapsulation, how long does it take to drain "almost" all the TNF-α out of the structure? We have to take this into consideration that we always have a *recovery* (total release amount) which is lower than the total TNF-α in the particles. Therefore, therapeutic dose must be defined regarding the recovery and release profile. In this work, therapeutic dose is constant amount of 5 µg. The release, depending on mechanism, continues up to the point that there is equilibrium between two regions (inside and outside of the particles) or/and when nanoparticles degrade or dissolve. TNF-α release was calculated as the percentage of TNF-α in the supernatant compared to original drug load. It has been tested via ELISA that the maximum released TNF-α amount from the individual tubes would be roughly 70% (up to 24h). While this recovery percentage for the same particles using the same tubes would be around 90% (up to 24h). A common way of describing these findings in Figure 18 is through the dissolution release mechanism. Dissolution occurs only when the medium around the nanoparticles is not saturated.[71] In this way, by refreshing the solvent at

each time point, the saturated layer is removed and replaced (same tubes). On the other hand, individual tubes are not refreshed in the same manner.

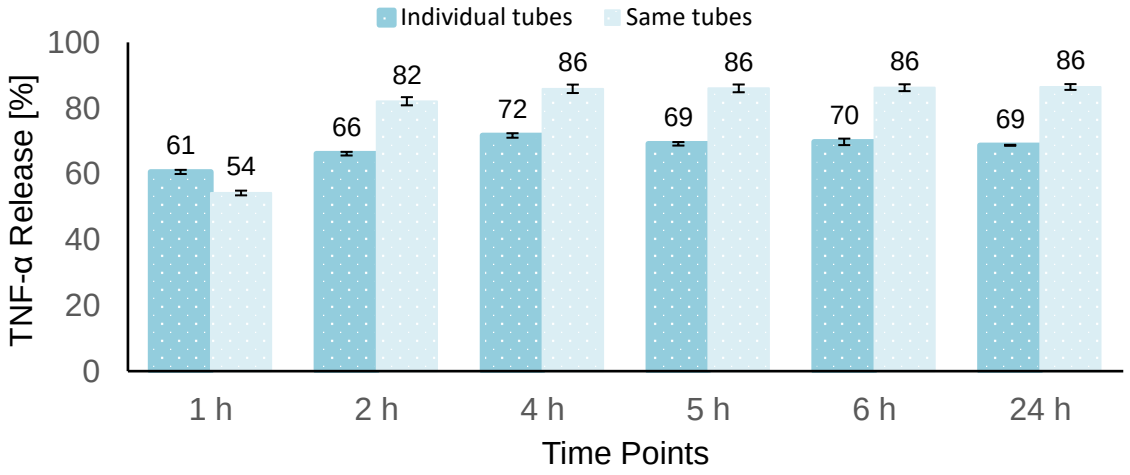

Figure 18. Comparing individual and same tube releases.

The recovery percentage for both the DMSN and $DMSN_{OPT}$ would be around 90% (up to 24h). Since an almost complete release is observed after 4 hours (Figure 19), a sustained release system is required for long-term release.

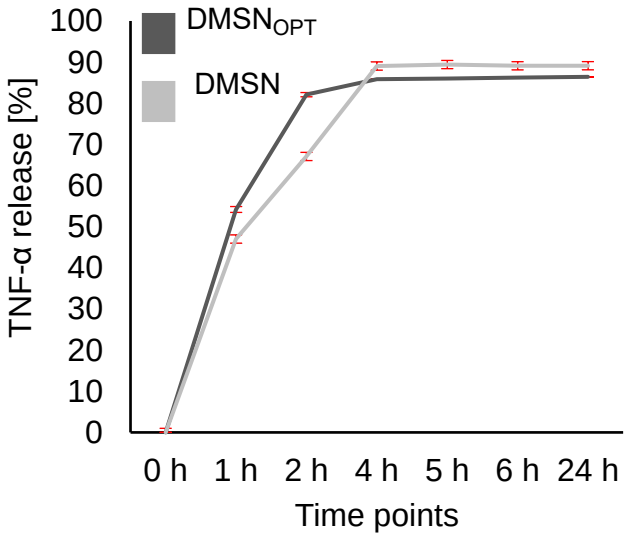

Figure 19. Recovery (total release amount) of DMSN and $DMSN_{OPT}$ up to 24 h.

4.6 Coating of the $DMSN_{OPT}$

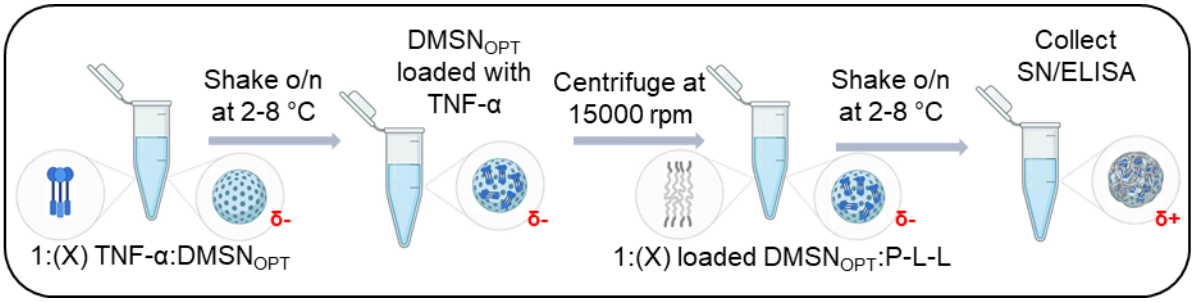

Figure 20. Schematic overview of the drug loading and coating process. Constant amount of TNF-α was incubated with $DMSN_{OPT}$ in different ratios (1:1-1:20) overnight and in PBS. Afterwards, supernatants were collected and TNF-α amount was determined via ELISA. TNF-α loaded $DMSN_{OPT}$ (1:20) were mixed this time with P-L-L in different ratios (1:1-1:6) at the same stated conditions for incubation. Coated TNF-α loaded $DMSN_{OPT}$ were washed twice and supernatants measured again.

Surface coatings of biomolecules on various mesoporous silica can influence their biomedical applications for a variety of reasons: (i) It can completely suppress the hemolytic effects of MSNs. It was observed that the hemolytic suppression was dependent on the protein concentrations in bare, aminated, and phosphonated MSNs. (ii) It can have drastic effects on cellular internalization. Thus, this can influence the biological behaviour of NPs, which can either be an advantage or a disadvantage; it can also lead to irreproducible biological studies. (iii) It can facilitate the crossing of the BBB due to the adsorption of alipoproteins. (iv) It may increase the uptake of particles by monocytes and macrophages when they are injected intravenously, which can greatly limit their therapeutic potential. (v) It can remove the targeting capabilities of surface-engineered nanoparticles. (vi) It can lower drug delivery efficiency, such as hydrophobic camptothecin anticancer drugs.[47]

The presence of abundant silanol groups makes functionalizing the surface of the particles relatively straightforward.[77] In this regard, one synthetic and one commercial polymer were studied. A specific biological environment can cause the NPs to undergo a variety of changes, such as the formation of a coating protein corona on its surface once plasma proteins are deposited there. Hence, it is essential to study the latest update on the 'synthetic identity' of NPs before they are tested biologically at the end of this step.[84]

4.6.1 Sarcosine-lsyine (synthetic). Sarcosine-lsyine is a polypeptoid-block-polypeptide copolymer which consists of 14 hydrophilic non-ionic sarcosine and 5

stimuli responsive ionic lysine monomers. The protein is biocompatible and stable in aqueous solution. Although the case of block copolymers is not typical of most adsorbing polymers, which are attached at many points along the chain, giving features known as trains, loops and tails.[85] The effective thickness of the adsorbed layer is more difficult to determine as the TEM images in Figure 21A and D confirm. It can be dominated by the tails, although these represent a very small proportion of the adsorbed amount. Here, even the lowest concentration of 20 µg/mL polymer causes effective flocculation. It is evident in Figure 21B that there is a significant loss of TNF-α after coating with 3- and 6-folds polymer (up to 50%). Additionally, the lowest polymer ratio (1:1) shows a burst release of up to 45% in the first few hours (Figure 21C).

A

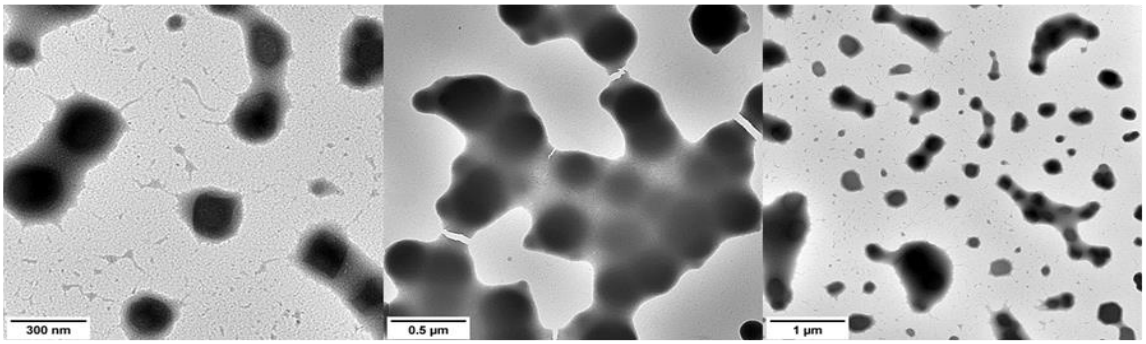

B

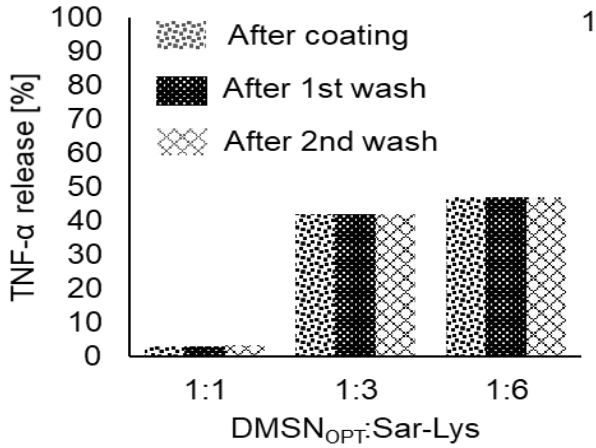

C

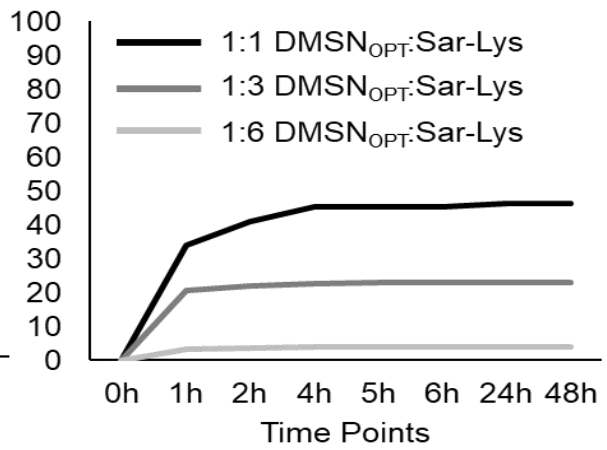

D

Ratio	Average zeta potential (mV)	Mean hydrodynamic size (nm)	PDI
1:1	-8.82	1000	0.27
1:3	-5.08	1928	0.24
1:6	+2.60	3222	0.28

Figure 21. Drug loading, release profile and coating of TNF-α loaded $DMSN_{OPT}$ with Sar-Lys. A) TEM images of coated TNF-α loaded $DMSN_{OPT}$. For visualization purposes, contrast of the polymer-particle complex was increased via staining. B) Displayed is the mean total TNF-α released during the coating process. For $DMSN_{OPT}$:Sar-Lys, low (1:1), medium (1:3) and high (1:6) ratios have been tested. C) Shown is the release of TNF-α after coating with different amount of polymer up to 48 h and in parallel. D) The table lists characteristics of coated TNF-α loaded $DMSN_{OPT}$. All measured values are averaged (n=3).

4.6.2 Poly-L-lysine (commercial). The effect of charge density and the concentration of the poly-L-lysine dispersion on coating characteristics were investigated.[55] Based on Figure 22, the affinity of P-L-L (positive amine) for silanol groups on the $DMSN_{OPT}$ surface (partial negative charge) decreased relatively when polymer concentration was increased. The kinetic washing steps confirm the irreversible adsorption interaction of P-L-L on silica.

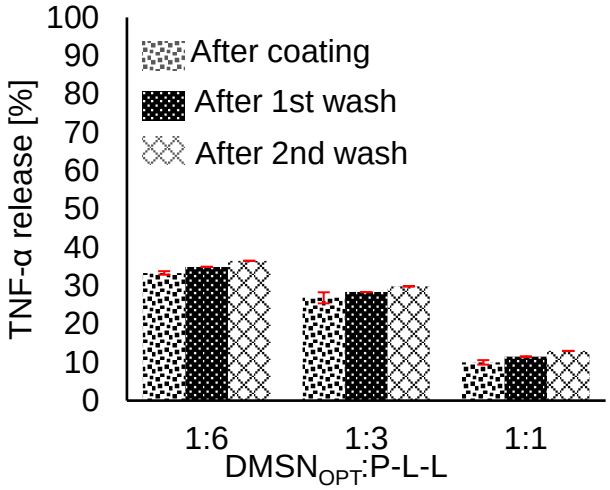

Figure 22. Mean total TNF-α released during the coating process. For $DMSN_{OPT}$:P-L-L, low (1:1), medium (1:3) and high (1:6) ratios were tested.

The release profile for different $DMSN_{OPT}$:P-L-L were very similar (±6%) (Figure 23). TNF-α release was greatly delayed (below 22% for up to 6 d). It appears that the loaded $DMSN_{OPT}$ is almost fully covered by P-L-L which opens up opportunities for long-term controlled release of drug for immunotherapy.[86,87]

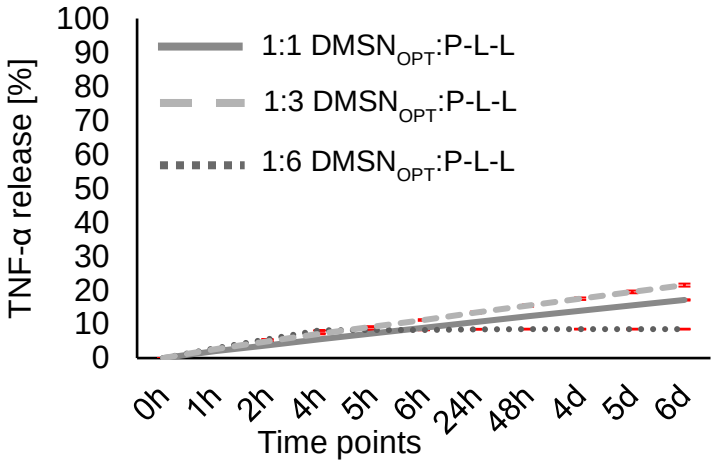

Figure 23. Sustained release of TNF-α after coating with different amount of polymer up to 6 d and in parallel.

The coating agent candidate is constituted of L-lysine, which exhibits a high positive charge under physiological conditions. A 1:1 ratio for DMSN$_{OPT}$:P-L-L was selected for further development of the coating process and shown to be best for the optimization of the coating process, since a) the loss of TNF-α during coating and washing is less (Figure 22), b) the final coated particles possess positive charge as shown in the characteristics (Table 4, suitable for electrostatic interaction with dendritic cell membrane), c) it is the lowest polymer amount used.

Table 4. Characteristics of Coated TNF-α loaded DMSN$_{OPT}$ for efficient coating. All the measured values are average (n=3).

Ratio	Average zeta potential (mV)	Mean hydrodynamic size (nm)	PDI
1:1	+16.40	673	0.21
1:3	-0.50	244	0.24
1:6	+16.43	375	0.27

Furthermore, TEM imaging proved no sufficient coating formation for 3:1 (3 times particles) and correlative DMSN$_{OPT}$ degradation after 4 h. It has also become evident that the process parameters such as shaking (particularly for TNF-α), temperature, medium and centrifugation speed (factors of diffusion) are relevant for the

reproducibility and quality of the coatings and the release profile of the encapsulated TNF-α. This study, for example, found that it was not applicable to effectively mix or dilute TNF-α within the plate (1:2) due to insufficient vortexing, and there can be no homogeneous solution. It is also relevant to note that sterically stabilised dispersions can be destabilised by changing the solvency of the medium for the stabilizing chains (polymer). Therefore, changing the coating and washing media from PBS to HEPES increased total released TNF-α by up to 15%. Following particle preparation and before the biological test, it is reasonable to keep the particles in the same solution.
The selected coated particles possess a charge of +16.40 mV. In addition, in Table 5, reproducibility of drug loading and coating operations are validated. 82±5 % of the primary TNF-α is accessible for administration.

Table 5. Batch to batch analysis for each presented step determined via ELISA for 1:20 TNF-α:DMSN$_{OPT}$ and 1:1 DMSN$_{OPT}$:P-L-L (n=3).

Batch	#1	#2	#3
Encapsulated TNF before coating (%)	99	98	98
Encapsulated Coated TNF (%)	90	80	85
Encapsulated+Coated+1Wash TNF (%)	88	78	83
Encapsulated+Coated+2Wash TNF (%)	**87**	**77**	**82**

With less steric stabilization effect of polymer, an individual chain can become attached to two or more particles, thus 'bridging' them together. In this way particles can form aggregates or attach to macroscopic surfaces to some extent even though they may be charged and repel each other (Figure 24). Considering the fact that kinetic factors also can increase the importance of bridging interactions. Very important: aggregates didn’t result in toxicity in cell viability assay for concentrations below 25 μg/mL earlier shown in Figure 12.

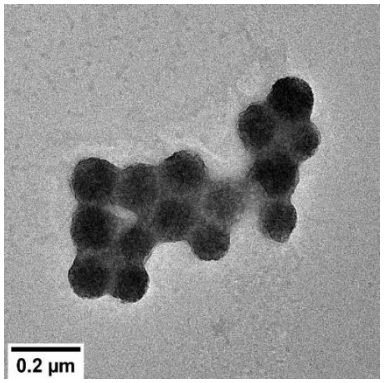

Figure 24. **Representative TEM image of coated TNF-α loaded DMSN$_{OPT}$.** For visualization purposes, contrast of the polymer-particle complex was increased by staining.

Specifically, researchers have found that ε-poly-L-lysine-functionalised MSNs are taken up efficiently by macrophage cells (most likely via endocytosis) and further reach autolysosomes where the polymer is degraded by lysosomal enzymes and the cargo is released.[47]

4.7 DCs maturation

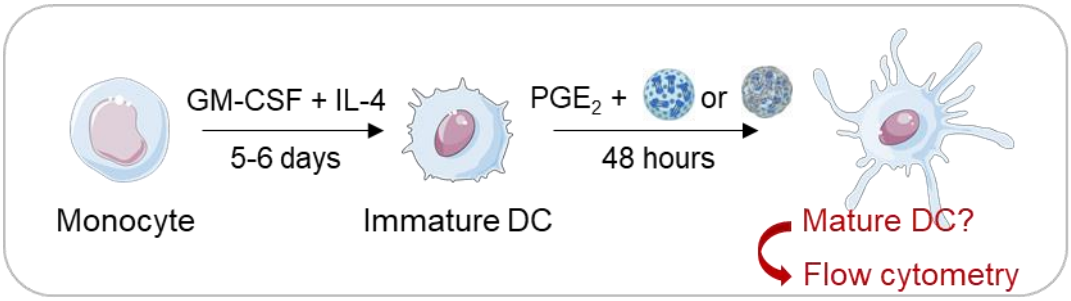

Figure 25. Schematic overview for the generation of human dendritic cells (DCs) and functional testing of uncoated and coated TNF-α-loaded DMSN$_{OPT}$ with human dendritic cells.

As one of the first cationic polymers that have been used as transfection agents, P-L-Ls are characterised by their intrinsic biodegradability and high charge density. In the current work, it is the focus to see the interaction of dendritic cells specifically with TNF-α loaded P-L-L coated DMSN$_{OPT}$ and the possibility of efficient endosome escape after endocytosis at physiological pH (detection of the particle followed by internalization process which in turn can liberate TNF-α from the complex).[56]

Researchers recently developed a nano-emulsion with L-phenylalanine-grafted P-L-L to encapsulate squalene as a potential adjuvant against influenza viruses, which could generate both cellular (Th1) and humoral (Th2) responses. The nano-emulsion showed excellent colloidal stability, good biocompatibility, and high squalene loading efficiency.[88]

As Kim's experiment showed, lipopolysaccharide (LPS), an agonist of TLR4, was added to the DCs at day 6 after isolation, and the cells were incubated for only 24 h. Based on optical images, with LPS treatment, DCs morphologically shifted from immature to mature, characterised by larger and longer pseudopodia and also, they expressed a high level of CD86 costimulatory molecule. Moreover, mature DCs had a less pronounced phagocytic ability compared to immature DCs.[15]

To induce DCs maturation in this study, skin inflammation was simulated. An example of this would be the addition of proinflammatory cytokines (like TNF-α) usually found during inflammation. Immature DCs that are stimulated following this protocol do not produce IL-12p70, a cytokine involved in T cell polarization and NK cell activation that

was thought to be crucial for proper anti-tumour T cell responses.[68] However, clinical trials applying this protocol for DCs maturation showed potent induction of cytotoxic tumour-reactive $CD8^+$ T cells and Th1 polarization in patients.

“During the first phase of early maturation up to 6 h after DCs activation the presence of a TLR ligand that is internalised together with the antigen promotes antigen cross-presentation. During the second phase of DCs maturation (between 7 and 20 h after activation), maturing DCs are still competent to take up certain antigens (immune complexes or bead-bound antigen, but not dead cells, for example) and to cross-present them with very high efficacy. During a final phase of maturation (after 20–24 h after DCs activation, depending on the type of DCs and stimulus), antigen cross-presentation is impaired”.[19]

To investigate the stimulation and activation of the immune system through DCs maturation (Figure 25) and T cell proliferation, nonadherent cells at day 5-6 of culture were transferred to 6-well plates in 3 mL culture medium ($0.75*10^6$-10^6 DC/well). Cells were stimulated with PGE_2 and/or TNF-α.The previous studies have shown the combination with TNF-α resulted in populations with a homogeneous DCs morphology as well as a comparable expression of CD83[89] while addition of PGE_2 alone had only little effect on morphology and phenotype of DCs. Therefore, we can display the distinguishable effect of TNF-α (if existing) in full DCs maturation. For this experiment, immature DCs, immature DCs+PGE_2 and immature DCs+PGE_2+TNF-α were cultured as controls for immature DCs+PGE_2+TNF-α loaded $DMSN_{OPT}$, and immature DCs+PGE_2+coated TNF-α loaded $DMSN_{OPT}$. Two more controls were added to investigate the activity of uncoated and coated $DMSN_{OPT}$: Immature DCs+PGE_2+ $DMSN_{OPT}$ and immature DCs+ PGE_2+empty coated $DMSN_{OPT}$. 48 hours later (after 24 h maturation was incomplete and insignificant), cells were assessed by morphology, phenotype and function. Control immature DCs are rounded and spherical (Figure 26, Φ), suggesting that the cells are mostly immature. As a result of maturation, DCs undergo a clear change in their morphology, have rough and boundless membranes and develop cellular extensions (dendrites) that enlarge cellular surface and eventually improve the interaction with T cells (Figure 26, +PGE_2, +PGE_2+TNF-α loaded $DMSN_{OPT}$).

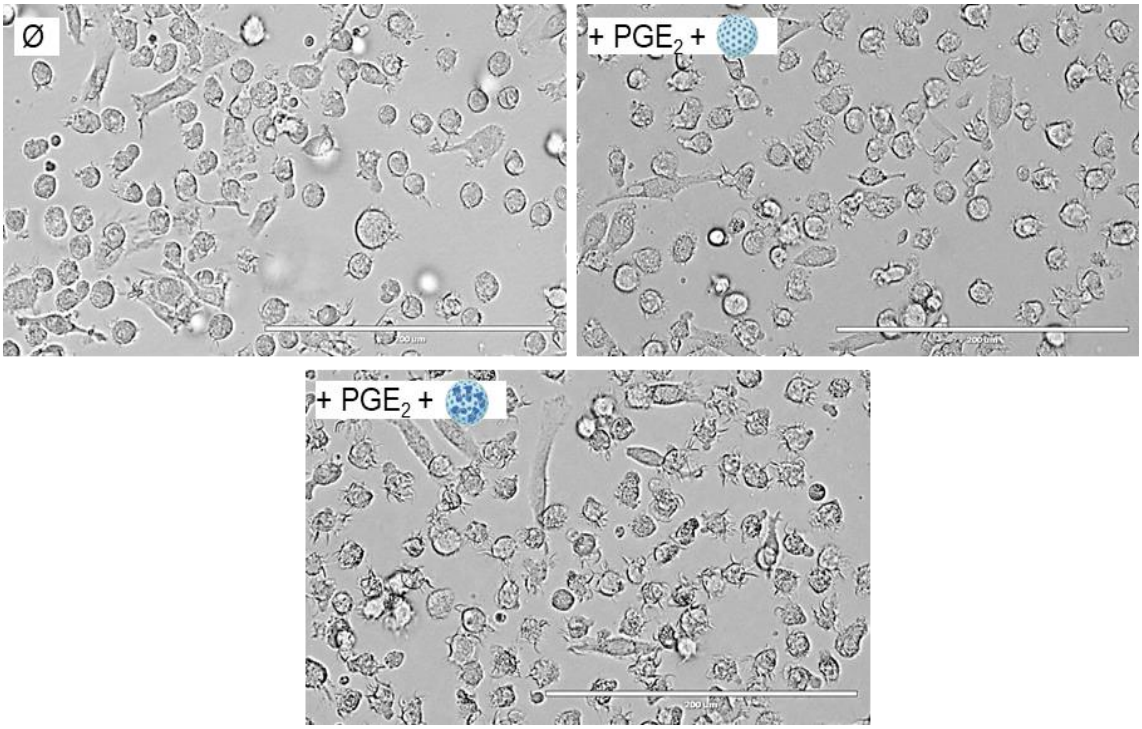

Figure 26. Light microscope images of human DCs cultured in cell culture medium. (X-VIVO 15 + GM-CSF/IL-4/plasma) + PGE_2 + empty vs. TNF-α-loaded $DMSN_{OPT}$ (uncoated particles). The images show cells at a 400x magnification.

As Figure 27 shows, immature DCs displayed low expression of CD80 and CD83 (below 4% in all the experiments). In general, addition of PGE_2 ± TNF-α leads to upregulation of CD80/83/86 compared to immature DCs. Contrary to the 20 to maximum 40% CD80 and CD83 upregulation with PGE_2 alone, addition of TNF-α significantly increased the expression up to more than 80%. It appears that both maturation markers behave identically.

Kienzle, Kurch, and colleagues used TNF-α and a cocktail insufficient for inducing full DCs maturation alone to demonstrate the immunostimulatory properties. While immature DCs displayed low expression of CD80 (9%) and CD83 (11%), expression of CD80 (36%) and CD83 (53%) was increased on DCs maturated with cytokines and TNF-α. DCs maturated with cytokines only and cytokines with empty DMSN displayed comparably weak and close levels of CD80 (14% and 12%, respectively) and CD83 upregulation (18% and 21%, respectively). TNF-α-loaded DMSN caused upregulation of CD80 (24%) and CD83 (38%) as well. Nevertheless, upregulation of the two maturation markers was not as noticeable as for free TNF-α, showing that DMSN delayed TNF-α's effects.[52]

Consequently, there must be a link between the results mentioned before and the structural differences between the pores. A small pore network (DMSN) might be a reason for TNF-α blocking. Meanwhile a bigger pore network ($DMSN_{OPT}$) liberates TNF-α more efficiently.

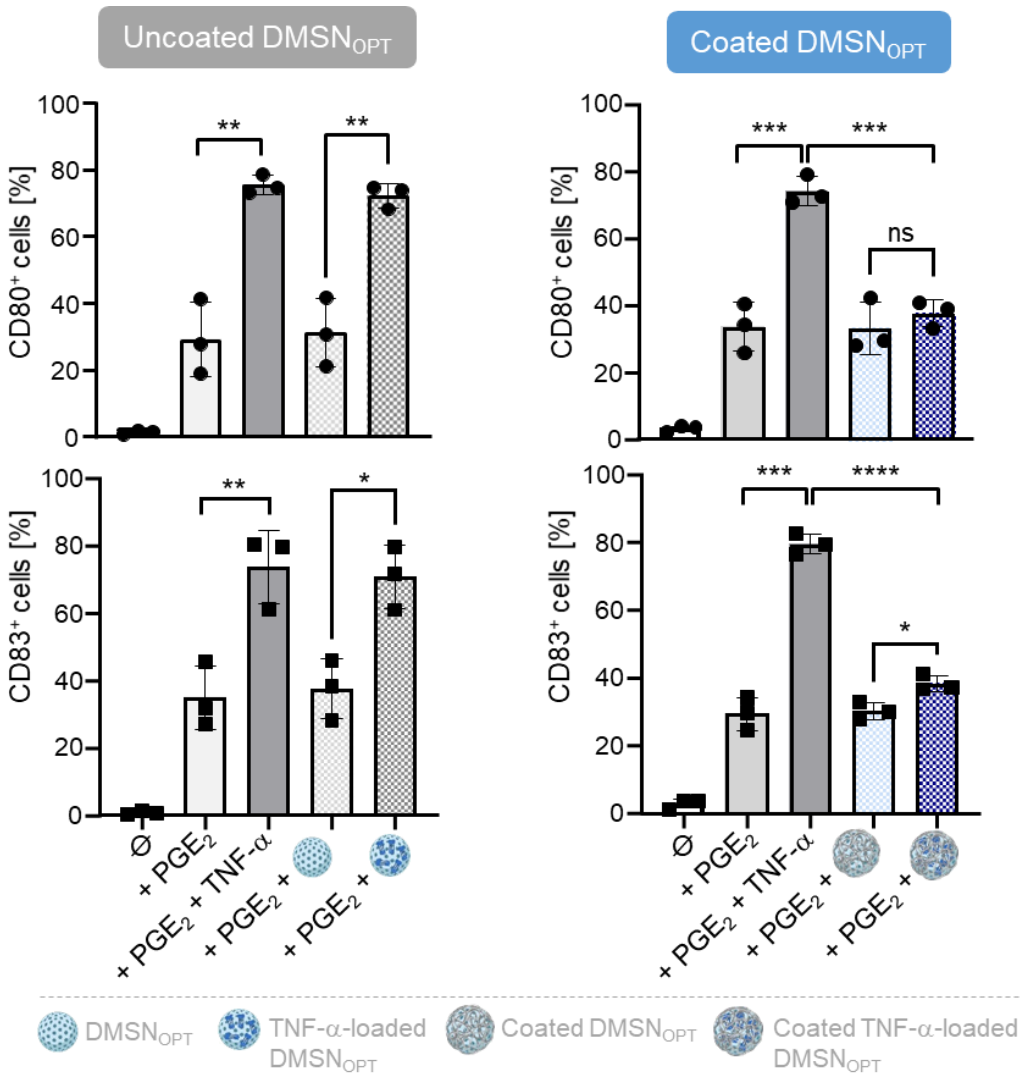

Figure 27. Flow cytometric analysis (CD80 & CD83) of DCs 48 h after incubation with different maturation cocktails. The average proportion ± SD of $CD80^+$ (top diagram) and $CD83^+$ (bottom diagram) cells (in %) from a total of n= 3 independent experiments is shown. Each symbol represents one individual donor. Left side displays the results for DCs maturation with uncoated TNF-α-loaded $DMSN_{OPT}$, in right side the corresponding results with coated TNF-α-loaded particles are shown. As a control for each experiment, DCs were incubated with PGE_2+ empty particles. Furthermore, immature DCs served as negative control. Statistical significance was determined using unpaired Student's t test relative to control group (as indicated). p-values of less than 0.05 were considered significant (* $p < 0.05$; ** $p < 0.01$; *** $p < 0.001$; **** $p < 0.0001$; ns = not significant).

Still, no difference was observed in CD86 expression when comparing PGE_2 ± TNF-α cultures (Figure 28). Since TNF-α loaded $DMSN_{OPT}$ caused the same effect as the free TNF-α control, we can conclude that TNF-α is successfully released from $DMSN_{OPT}$. In contrast, TNF-α is not released from coated $DMSN_{OPT}$ confirming our hypothesis that coating delays the release during the specified span of 48 h, and TNF-α has not become free via phagocytosis (due to the larger diameter of coated nanoparticles, the process is referred to as phagocytosis [34]). The parallel test of the supernatants *via* ELISA also validated the findings. No TNF-α was found in any of the supernatants of coated TNF-α loaded $DMSN_{OPT}$. Uncoated and coated $DMSN_{OPT}$ alone has no stimulatory effect on characteristic DCs surface markers. Having this feature makes them reliable and suitable for application as immune carrier system.

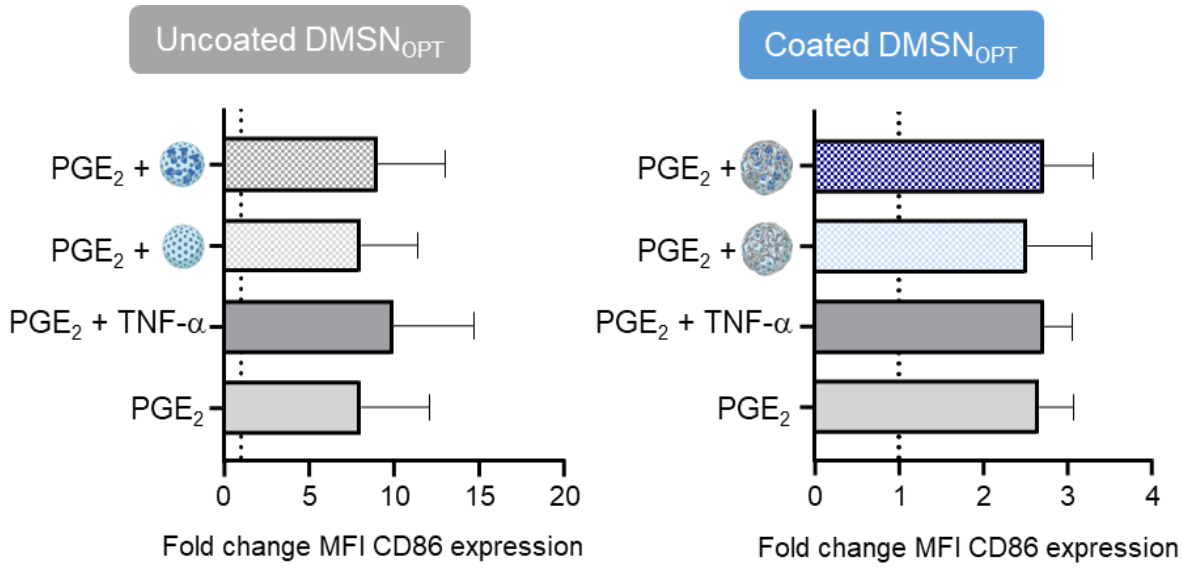

Figure 28. Flow cytometric analysis (CD86) of DCs 48 h after incubation with different maturation cocktails. Fold change in mean fluorescence intensity (MFI) of CD86 expression of mature DCs is depicted normalised to the MFI CD86 expression of the corresponding immature DCs culture. The left side displays the results for DCs maturation with uncoated TNF-α-loaded $DMSN_{OPT}$, the right side shows the corresponding results with coated TNF-α-loaded particles.

4.8 T cell proliferation

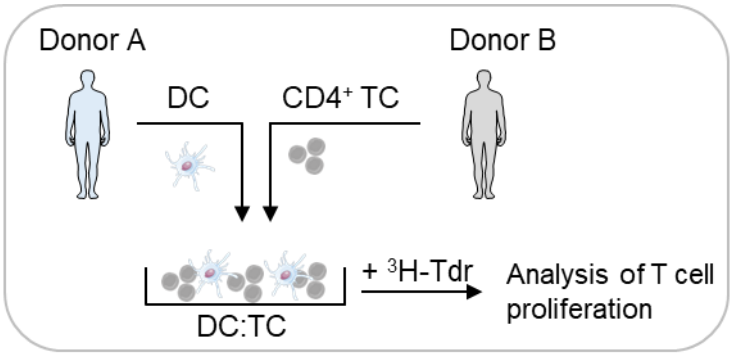

Figure 29. Schematic overview of Mixed Leukocyte Reaction (MLR). Differently treated/matured DCs from donor A are cocultured with CD4+ T cells, isolated from the peripheral blood of an independent donor B, at different DC:TC ratios (1:10 to 1:640). After four days, T cell proliferation is determined via incorporation of 3H-thymidine (3H-Tdr).

Increased expression of costimulatory molecules is associated with a higher capacity to stimulate T cells which can be tested *via* MLR (Figure 29). In general, DCs treated with PGE_2+TNF-α have a higher stimulatory capacity than DCs treated with PGE_2 alone resulting a higher TC proliferation (Figure 30A+B). The stimulatory ability of PGE_2+TNF-α and PGE_2+TNF-α loaded $DMSN_{OPT}$ in the given range of DC:TC are equivalent. This study focused on the impact of DC:TC with constant DCs numbers. The maximum T cell proliferation provoked by fully matured DCs (either with free or TNF-α loaded $DMSN_{OPT}$) is achieved at 1:10. For a higher number of T cells a declining trend was observed, while T cell escalation at 1:640 results in almost an inhibition of proliferation. Cumulative data of 3 individual donors show a significant difference in the stimulatory capacity of DCs when comparing uncoated TNF-α loaded $DMSN_{OPT}$ to coated TNF-α loaded $DMSN_{OPT}$ (Figure 30, C). Coated TNF-α loaded $DMSN_{OPT}$ do not release TNF-α resulting in less maturation of DCs and thus less TC proliferation which indicates successful coating.

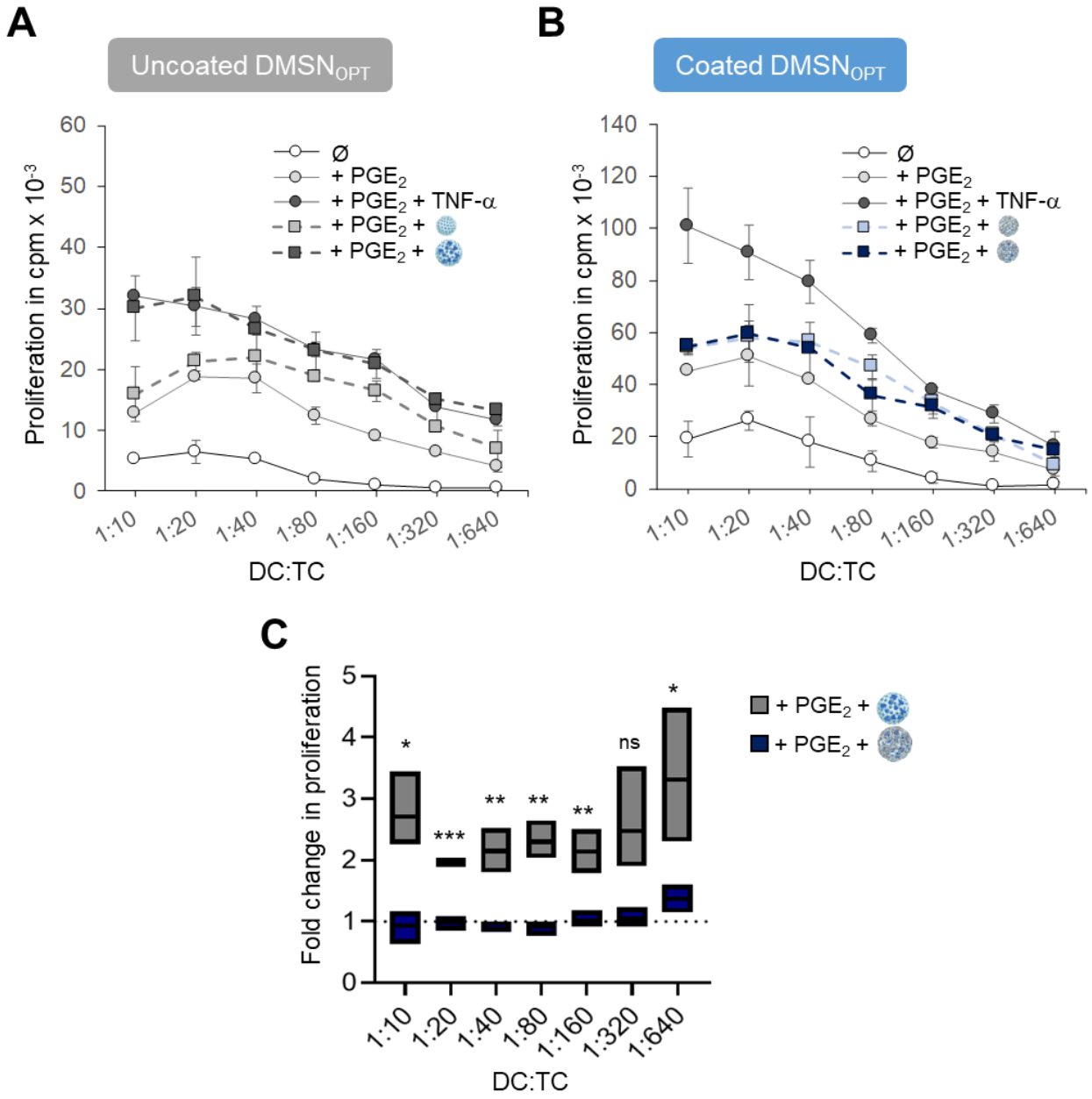

Figure 30. Immunostimulatory capacity of human DCs cultured with uncoated vs. coated TNF-α-loaded DMSN$_{OPT}$. A+B) The curve diagrams summarise T cell proliferation displayed as mean counts per minute (cpm) ± standard deviation (SD) of triplicates. One representative experiment out of 3 is shown. A displays the results for DCs maturation with uncoated TNF-α-loaded DMSN$_{OPT}$, in B the corresponding results with coated TNF-α-loaded particles are shown. C) Box diagram displays fold change T cells stimulated with DCs, which were matured with TNF-α-loaded DMSN$_{OPT}$ (uncoated vs. coated), is normalised to the respective control setup including empty DMSN$_{OPT}$. Results are shown as a mean of three independent experiments. Statistical significance was determined using unpaired Student's t test relative to the corresponding control group/DC:TC ratio (as indicated). * $p < 0.05$; ** $p < 0.01$, *** $p < 0.001$; ns = not significant.

4.9 Immunological activity of $DMSN_{OPT}$

There have been reports that NPs inhibit DCs maturation. For instance, in porcine Mo-DCs stimulated and treated with LPS + negatively charged QD655-COOH (18 nm), expression of CD80/CD86 was suppressed.[90] Gold nanoparticles with a diameter of 10 nm inhibited the expression of CD86, CD83, and IL-12p70 in human DCs in response to LPS treatment.[91] NPs should be investigated further so that side effects of use in cancer immunotherapy can be avoided. In all experiments, the possible inhibitory characteristics of both the empty and empty coated $DMSN_{OPT}$ were evaluated. When PGE_2 media with or without particles are compared, no impact was detected on the stimulation/inhibition of NPs alone. Since the expression of surface markers is the same in PGE_2 plus TNF-α media with or without NPs, the same conclusion can be drawn.

Empty nanoparticles were used in a separate experiment to examine DCs maturation and T cell proliferation (including controls). The question is whether these empty particles have any impact on the response, and how much error may be induced by the results. Ultimately, empty $DMSN_{OPT}$ had no stimulatory capacity and is thus inert (Figure 30).

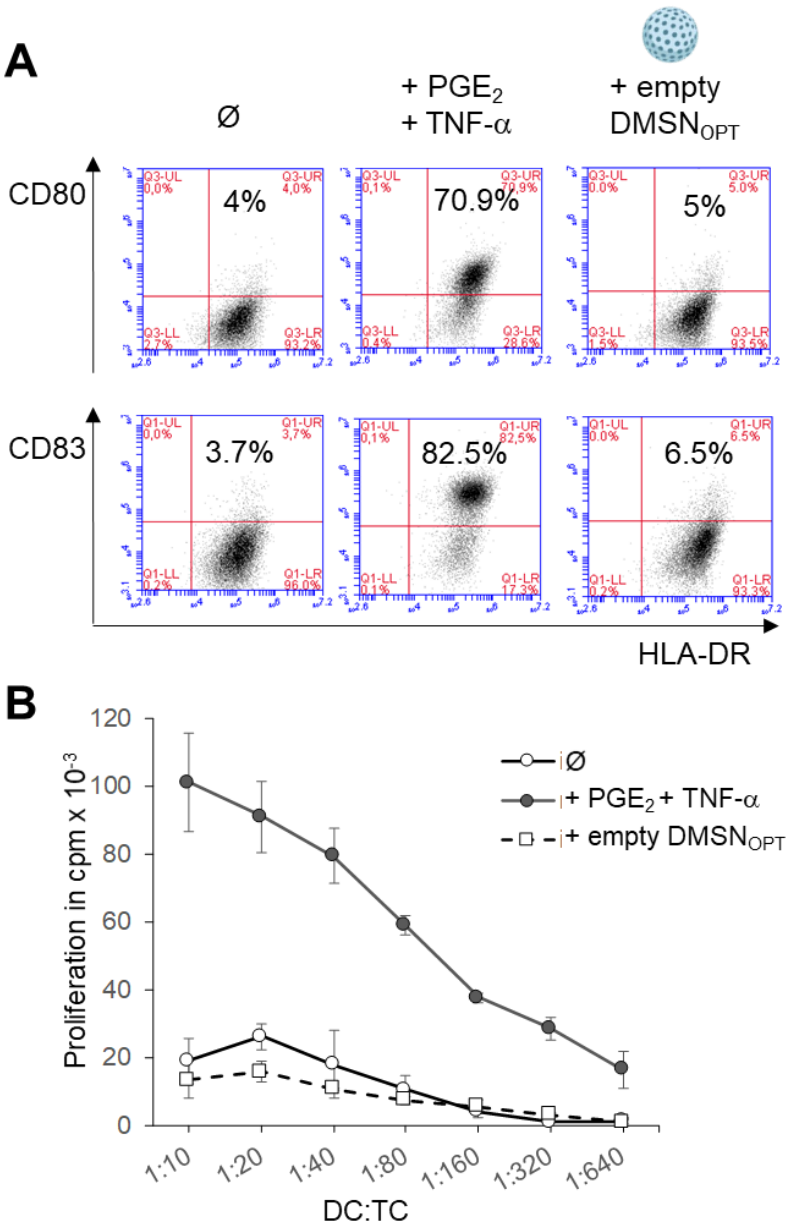

Figure 31. DMSN$_{OPT}$ is inert and has no immunostimulatory capacity. A) Flow cytometric analysis of human DCs incubated with empty DMSN$_{OPT}$ for 48 h. Dot plots show the percentage of CD80 and CD83 expressing DCs. One representative result out of n = 3 independent experiments is shown. B) Immunostimulatory capacity of DCs treated with empty DMSN$_{OPT}$ (MLR setting): Curve diagram summarises T cell proliferation displayed as mean counts per minute (cpm) ± standard deviation (SD) of triplicates. One representative experiment out of 3 is shown.

5 Conclusion

I have designed, prepared and characterised $DMSN_{OPT}$, using the amino acid-based polymer P-L-L as gate keeper model with a TNF-α encapsulation efficiency of 82±5%. Extensive investigations were carried out on the reproducibility of the preparation and characterization of the $DMSN_{OPT}$, release of TNF-α with and without coating, as well as the interactions of TNF-α with $DMSN_{OPT}$, polymer and dendritic cells. Appropriate ratio/concentration of the $DMSN_{OPT}$ in the efficient system was determined. Application of the polymer as a coating agent achieved a controlled/cell-specific release of TNF-α, which is being tested for activation of adaptive immunity. Coated loaded $DMSN_{OPT}$ did not show any maturation of the dendritic cells or T cell proliferation in contrast to the uncoated loaded $DMSN_{OPT}$. This shows and confirms that the achieved coating according to the developed procedures is firm and does not release any TNF-α under the selected conditions. Lastly, TNF-α was successfully released from $DMSN_{OPT}$ and showed the same effect as a free TNF-α control.

6 Perspectives

Encapsulation of drugs within nanocarriers that selectively target malignant cells promises to mitigate side effects of conventional chemotherapy and to enable delivery of the unique drug combinations needed for personalised medicine. Even though the intracellular delivery of several drugs in animal cells by mesoporous silica materials has been achieved, there are still many unsettled questions for future practical applications, such as biodistribution, the acute and chronic toxicities, long-term stability, circulation properties and targeting efficacy in vivo.[92]

Targeted delivery of TNF-α encapsulated within mesoporous silica-based materials as developed, optimised and reported here can overcome problems exhibited by conventional free TNF-α including limited stability, rapid clearing and in particular, lack of selectivity which results in nonspecific toxicity to normal cells and prevents the dose escalation. Therefore, the following selective targeting strategies of the $DMSN_{OPT}$ with the encapsulated TNF-α may be employed:

1) Functionalisation of the $DMSN_{OPT}$

Ligands on the surface of the $DMSN_{OPT}$ that are specific to dendritic cell receptors. They will interact with the receptors expressed on the cells to promote the $DMSN_{OPT}$ binding and internalization.

Multiple copies of a targeting ligand can be conjugated to the nanocarrier surface to promote multivalent binding effects. However, high ligand densities can promote nonspecific interactions with endothelial and other unobjective cells and increase immunogenicity, resulting in opsonization-mediated clearance of nanocarriers.[92,93]

2) Modification of the $DMSN_{OPT}$ surface

Similarly to what is reported here, coated nanoparticles can be prepared with different polymers and techniques. Also, ligands could be added to functionalise them. For example, one of the advantages of P-L-L is its side chain functionality which could be optimised for the preferable release kinetics and targeting depending on the application (Increasing circulation time by reducing interactions with serum proteins and inhibiting phagocyte uptake, for example).[94]

3) Encapsulation of $DMSN_{OPT}$-TNF-α in liposomes and lipid nanoparticles (Protocell)

To address the multiple challenges of targeted delivery, a new class of nanocarrier is being developed that combines mesoporous silica particles and liposomes. Fusion of liposomes to a spherical, high-surface-area, nanoporous silica core, followed by modification of the resulting supported lipid bilayer (SLB) with multiple copies of a targeting peptide, a fusogenic peptide and PEG results in a nanocarrier construct (the 'protocell') that, compared with liposomes, the most extensively studied class of nanocarriers improves on capacity, selectivity and stability and enables targeted delivery and controlled release of high concentrations of multicomponent cargos within the cytosol of cancer cells.[92]

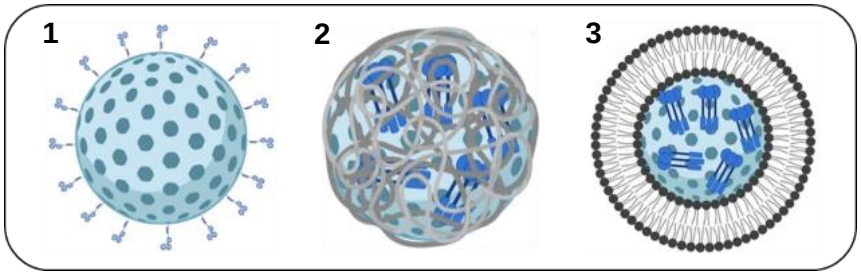

Figure 32. A selection of targeting strategies for $DMSN_{OPT}$ with TNF-α encapsulated.

7 References

1. Teli, M. K., Mutalik, S. & Rajanikant, G. K. *Nanotechnology and Nanomedicine: Going Small Means Aiming Big*. *Curr. Pharm. Design*, **16**, 1882-1892 (2010).

2. Sercombe, L., Veerati, T., Moheimani, F., Wu, S. Y., Sood, A. K., & Hua, S. Advances and challenges of liposome assisted drug delivery. *Front. Pharmacol.* **6**, 286 (2015).

3. Hare, J. I., Lammers, T., Ashford, M. B., Puri, S., Storm, G., & Barry, S. T. Challenges and strategies in anti-cancer nanomedicine development: An industry perspective. *Adv. Drug Deliv. Rev.* **108**, 25–38 (2017).

4. Hua, S., de Matos, M. B. C., Metselaar, J. M. & Storm, G. Current trends and challenges in the clinical translation of nanoparticulate nanomedicines: Pathways for translational development and commercialization. *Front. Pharmacol.* **9**, 790 (2018).

5. Talekar, M., Tran, T. H. & Amiji, M. Translational Nano-Medicines: Targeted Therapeutic Delivery for Cancer and Inflammatory Diseases. *AAPS J.* **17**, 813–827 (2015).

6. Larsson, M., Huang, W. T., Liu, D. M. & Losic, D. Local co-administration of gene-silencing RNA and drugs in cancer therapy: State-of-the art and therapeutic potential. *Cancer Treat. Rev.* **55**, 128–135 (2017).

7. Gonzalez-Valdivieso, J., Girotti, A., Schneider, J. & Arias, F. J. Advanced nanomedicine and cancer: Challenges and opportunities in clinical translation. *Int. J. Pharm.* **599,** 120438 (2021).

8. Luxenhofer, R., Barz, M. & Schillmeier, M. Quo vadis nanomedicine? *Nanomedicine* **9**, 2083–2086 (2014).

9. Bobo, D., Robinson, K. J., Islam, J., Thurecht, K. J. & Corrie, S. R. Nanoparticle-Based Medicines: A Review of FDA-Approved Materials and Clinical Trials to Date. *Pharm. Res.* **33**, 2373–2387 (2016).

10. Galmarini, S., Hanusch, U., Giraud, M., Cayla, N., Chiappe, D., von Moos, N., Hofmann, H. & Maurizi, L. "Beyond unpredictability: the importance of

reproducibility in understanding the protein corona of nanoparticles." *Bioconj. Chem.* **29** (10), 3385-3393 (2018).

11. Halwani, A. A. Development of Pharmaceutical Nanomedicines: From the Bench to the Market. *Pharmaceutics* **14**, 106 (2022).

12. Tran, S., DeGiovanni, P., Piel, B. & Rai, P. Cancer nanomedicine: a review of recent success in drug delivery. *Clin. and Transl. Med.* **6**, 44 (2017).

13. Tang, T., Eldabaje, R. and Yang, L. Current status of biological therapies for the treatment of metastatic melanoma. *Anticancer Res.* **36** (7), 3229-3241 (2016).

14. Patente, T. A., Pinho, M. P., Oliveira, A. A., Evangelista, G., Bergami-Santos, P. C., & Barbuto, J. A. Human dendritic cells: Their heterogeneity and clinical application potential in cancer immunotherapy. *Front. Immunol.* **10**, 3176 (2019).

15. Kim, M. K. & Kim, J. Properties of immature and mature dendritic cells: phenotype, morphology, phagocytosis, and migration. *RSC Adv.* **9**, 11230–11238 (2019).

16. Banchereau, J. & Steinman, R. M. *Dendritic cells and the control of immunity*. *Nature* 392, 245-252 (1998).

17. Matzinger, P. *The Danger Model: A Renewed Sense of Self*. www.sciencemag.org. *Science.* **296**. 301-305 (2002).

18. Winzler, C., Rovere, P., Rescigno, M., Granucci, F., Penna, G., Adorini, L., Zimmermann, V. S., Davoust, J. & Ricciardi-Castagnoli, P. Maturation Stages of Mouse Dendritic Cells in Growth Factor-dependent Long-Term Cultures. *J. Exp. Med.* **185**, 317-328 http://rupress.org/jem/article-pdf/185/2/317/1110244/5369.pdf (1997).

19. Alloatti, A., Kotsias, F., Magalhaes, J. G., & Amigorena, S. Dendritic cell maturation and cross-presentation: timing matters!. *Immunological reviews*, ***272***, 97-108 (2016).

20. Haniffa, M., Gunawan, M. & Jardine, L. Human skin dendritic cells in health and disease. *J. Dermatol. Sci.* **77**, 85–92 (2015).

21. Capini, C., Jaturanpinyo, M., Chang, H. I., Mutalik, S., McNally, A., Street, S., Steptoe, R., O'Sullivan, B., Davies, N. & Thomas, R. Antigen-Specific Suppression of Inflammatory Arthritis Using Liposomes. *J. Immunol.* **182**, 3556–3565 (2009).

22. White, K. L., Rades, T., Furneaux, R. H., Tyler, P. C. & Hook, S. Mannosylated liposomes as antigen delivery vehicles for targeting to dendritic cells. *J. Pharm. Pharmacol.* **58**, 729–737 (2010).

23. Getts, D. R., Shea, L. D., Miller, S. D. & King, N. J. C. Harnessing nanoparticles for immune modulation. *Trends Immunol.* **36**, 419–427 (2015).

24. Dane, K. Y., Nembrini, C., Tomei, A. A., Eby, J. K., O'Neil, C. P., Velluto, D., Swartz, M. A., Inverardi, L. & Hubbell, J. A. Nano-sized drug-loaded micelles deliver payload to lymph node immune cells and prolong allograft survival. *J. Control. Release* **156**, 154–160 (2011).

25. Fornaguera, C., Guerra-Rebollo, M., Angel Lazaro, M., Castells-Sala, C., Meca-Cortés, O., Ramos-Pérez, V., Cascante, A., Rubio, N., Blanco, J. & Borrós, S. mRNA Delivery System for Targeting Antigen-Presenting Cells In Vivo. *Adv. Healthcare Mater.* **7**, 1800335 (2018).

26. Fytianos, K., Rodriguez-Lorenzo, L., Clift, M. J., Blank, F., Vanhecke, D., Von Garnier, C., Petri-Fink, A. & Rothen-Rutishauser, B. Uptake efficiency of surface modified gold nanoparticles does not correlate with functional changes and cytokine secretion in human dendritic cells in vitro. *Nanomed.: Nanotechnol., Biol., Med.* **11**, 633–644 (2015).

27. Arosio, D., Chiodo, F., Reina, J. J., Marelli, M., Penadés, S., van Kooyk, Y., García-Vallejo, J. J. & Bernardi, A. Effective targeting of DC-sign by α-fucosylamide functionalized gold nanoparticles. *Bioconj. Chem.* **25**, 2244–2251 (2014).

28. Stead, S. O., McInnes, S. J., Kireta, S., Rose, P. D., Jesudason, S., Rojas-Canales, D., Warther, D., Cunin, F., Durand, J., Drogemuller, C. J., Carroll, R. P., Coates, P. T. & Voelcker, N. H. Manipulating human dendritic cell phenotype and function with targeted porous silicon nanoparticles. *Biomaterials* **155**, 92–102 (2018).

29. Stead, S. O., Kireta, S., McInnes, S. J., Kette, F. D., Sivanathan, K. N., Kim, J., Cueto-Diaz, E. J., Cunin, F., Durand, J., Drogemuller, C. J., Carroll, R. P., Voelcker, N. H. & Coates, P. T. Murine and Non-Human Primate Dendritic Cell Targeting Nanoparticles for in Vivo Generation of Regulatory T-Cells. *ACS Nano* **12**, 6637–6647 (2018).

30. Heidegger, S., Gößl, D., Schmidt, A., Niedermayer, S., Argyo, C., Endres, S., Bein, T. & Bourquin, C. Immune response to functionalized mesoporous silica nanoparticles for targeted drug delivery. *Nanoscale* **8**, 938–948 (2016).

31. Urbanavicius, D., Alvarez, T., Such, G. K., Johnston, A. P. R. & Mintern, J. D. The potential of nanoparticle vaccines as a treatment for cancer. *Mol. Immunol.* **98**, 2–7 (2018).

32. Zupančič, E., Curato, C., Paisana, M., Rodrigues, C., Porat, Z., Viana, A. S., Afonso, C. A.M., Pinto, J., Gaspar, R., Moreira, J. N., Satchi-Fainaro, R., Jung, S. & Florindo, H. F. Rational design of nanoparticles towards targeting antigen-presenting cells and improved T cell priming. *J. Control. Release* **258**, 182–195 (2017).

33. Bachmann, M. F. & Jennings, G. T. Vaccine delivery: A matter of size, geometry, kinetics and molecular patterns. *Nature Rev. Immunol.* **10**, 787–796 (2010).

34. Manolova, V., Flace, A., Bauer, M., Schwarz, K., Saudan, P., & Bachmann, M. F. Nanoparticles target distinct dendritic cell populations according to their size. *Eur. J. Immunol.* **38**, 1404–1413 (2008).

35. Rincon-Restrepo, M., Mayer, A., Hauert, S., Bonner, D. K., Phelps, E. A., Hubbell, J. A., & Hirosue, S. Vaccine nanocarriers: Coupling intracellular pathways and cellular biodistribution to control CD4 vs CD8 T cell responses. *Biomaterials* **132**, 48–58 (2017).

36. Shima, F., Uto, T., Akagi, T., Baba, M. & Akashi, M. Size effect of amphiphilic poly(γ-glutamic acid) nanoparticles on cellular uptake and maturation of dendritic cells in vivo. *Acta Biomater.* **9**, 8894–8901 (2013).

37. Landgraf, M., Lahr, C. A., Kaur, I., Shafiee, A., Sanchez-Herrero, A., Janowicz, P. W., & Hutmacher, D. W. Targeted camptothecin delivery via silicon nanoparticles reduces breast cancer metastasis. *Biomaterials* **240**, 119791 (2020).

38. Porter, C. J. H. & Trevaskis, N. L. Targeting immune cells within lymph nodes. *Nature Nanotechnol.* **15**, 423–425 (2020).

39. Mates, J. M., Yao, Z., Cheplowitz, A. M., Suer, O., Phillips, G. S., Kwiek, J. J., & Anderson, C. L. Mouse liver sinusoidal endothelium eliminates HIV-like particles from blood at a rate of 100 million per minute by a second-order kinetic process. *Front. Immunol.* **8**, 35 (2017).

40. Kumar, S., Anselmo, A. C., Banerjee, A., Zakrewsky, M., & Mitragotri, S. Shape and size-dependent immune response to antigen-carrying nanoparticles. *J. of Control. Release* **220**, 141–148 (2015).

41. Niikura, K., Matsunaga, T., Suzuki, T., Kobayashi, S., Yamaguchi, H., Orba, Y., & Sawa, H. Gold nanoparticles as a vaccine platform: Influence of size and shape on immunological responses in vitro and in vivo. *ACS Nano* **7**, 3926–3938 (2013).

42. Cifuentes-Rius, A., de Puig, H., Kah, J. C. Y., Borros, S. & Hamad-Schifferli, K. Optimizing the properties of the protein corona surrounding nanoparticles for tuning payload release. *ACS Nano* **7**, 10066–10074 (2013).

43. Johnston, B. D., Kreyling, W. G., Pfeiffer, C., Schäffler, M., Sarioglu, H., Ristig, S., & Parak, W. J. Colloidal Stability and Surface Chemistry Are Key Factors for the Composition of the Protein Corona of Inorganic Gold Nanoparticles. *Adv. Funct. Mater.* **27**, 1701956 (2017).

44. Lundqvist, M., Stigler, J., Elia, G., Lynch, I., Cedervall, T., & Dawson, K. A. *Nanoparticle size and surface properties determine the protein corona with possible implications for biological impacts*. www.pnas.org/cgi/content/full/ (2008). *Proc. Natl. Acad. Sci. U.S.A.* **105**, 14265-14270 (2008)

45. Kurch, S. A. *Mesoporous Silica Nanoparticle for Drug Delivery of Cancer Therapeutics*. Johannes Gutenberg University; 2018.

46. Vallet-Regí, M., Colilla, M., Izquierdo-Barba, I. & Manzano, M. Mesoporous silica nanoparticles for drug delivery: Current insights. *Molecules* **23**, 47 (2018).

47. Croissant, J. G., Fatieiev, Y., Almalik, A. & Khashab, N. M. Mesoporous Silica and Organosilica Nanoparticles: Physical Chemistry, Biosafety, Delivery Strategies, and Biomedical Applications. *Adv. Healthcare Mater.* **7**, 1700831 (2018).

48. Yang, P., Gai, S. & Lin, J. Functionalized mesoporous silica materials for controlled drug delivery. *Chem. Soc. Rev.* **41**, 3679–3698 (2012).

49. Phillips, E., Penate-Medina, O., Zanzonico, P. B., Carvajal, R. D., Mohan, P., Ye, Y., Humm, J., Gönen, M., Kalaigian, H., Schöder, H., Strauss, H. W., Larson, S. M. Wiesner, U. & Bradbury, M. S. Clinical translation of an ultrasmall inorganic optical-PET imaging nanoparticle probe. *Science translational medicine*, **6**, 260ra149-260ra149 (2014).

50. Anselmo, A. C. & Mitragotri, S. Nanoparticles in the clinic: An update post COVID-19 vaccines. *Bioeng. Transl. Med.* **6**, e10246 (2021).

51. Yang, Y., Zhang, M., Song, H. & Yu, C. Silica-Based Nanoparticles for Biomedical Applications: From Nanocarriers to Biomodulators. *Acc. Chem. Res.* **53**, 1545–1556 (2020).

52. Kienzle, A., Kurch, S., Schlöder, J., Berges, C., Ose, R., Schupp, J., & Jonuleit, H. Dendritic Mesoporous Silica Nanoparticles for pH-Stimuli-Responsive Drug Delivery of TNF-Alpha. *Adv. Healthcare Mater.* **6**, 1700012 (2017).

53. Xu, C., Yu, M., Noonan, O., Zhang, J., Song, H., Zhang, H., & Yu, C. Core-Cone Structured Monodispersed Mesoporous Silica Nanoparticles with Ultra-large Cavity for Protein Delivery. *Small* **11**, 5949–5955 (2015).

54. Cha, B. G., Jeong, J. H. & Kim, J. Extra-Large Pore Mesoporous Silica Nanoparticles Enabling Co-Delivery of High Amounts of Protein Antigen and Toll-like Receptor 9 Agonist for Enhanced Cancer Vaccine Efficacy. *ACS Central Sci.* **4**, 484–492 (2018).

55. Francoia, J. P. & Vial, L. Everything You Always Wanted to Know about Poly-l-lysine Dendrigrafts (But Were Afraid to Ask). *Chem. Eur. J.* **24**, 2806–2814 (2018).

56. Zheng, M., Pan, M., Zhang, W., Lin, H., Wu, S., Lu, C., & Cai, J. Poly(α-L-lysine)-based nanomaterials for versatile biomedical applications: Current advances and perspectives. *Bioact. Mater.* **6**, 1878–1909 (2021).

57. Nandiyanto, A. B. D., Kim, S. G., Iskandar, F. & Okuyama, K. Synthesis of spherical mesoporous silica nanoparticles with nanometer-size controllable pores and outer diameters. *Micropor. Mesopor. Mater.* **120**, 447–453 (2009).

58. Gustafsson, H., Isaksson, S., Altskär, A. & Holmberg, K. Mesoporous silica nanoparticles with controllable morphology prepared from oil-in-water emulsions. *J. Coll. Interf. Sci.* **467**, 253–260 (2016).

59. Shen, D., Yang, J., Li, X., Zhou, L., Zhang, R., Li, W., & Zhao, D. Biphase stratification approach to three-dimensional dendritic biodegradable mesoporous silica nanospheres. *Nano Lett.* **14**, 923–932 (2014).

60. Dang, M., Li, W., Zheng, Y., Su, X., Ma, X., Zhang, Y., & Wang, L. Mesoporous organosilica nanoparticles with large radial pores via an assembly-reconstruction process in bi-phase. *J. Mater. Chem. B* **5**, 2625–2634 (2017).

61. Walsh, L. J., Trinchierit, G., Waldorf, H. A., Whitaker, D. & Murphy, G. F. *Human dermal mast cells contain and release tumour necrosis factor a, which induces endothelial leukocyte adhesion molecule 1 (skin/cytokines/endothelium/inflammation)*. *Proc. Natl. Acad. Sci. U.S.A.* **88** 4220-4224 (1991).

62. Swardfager, W., Lanctôt, K., Rothenburg, L., Wong, A., Cappell, J., & Herrmann, N. A meta-analysis of cytokines in Alzheimer's disease. *Biological Psychiatry* **68**, 930–941 (2010).

63. Uzzan, S. & Azab, A. N. Anti-tnf-α compounds as a treatment for depression. *Molecules* **26**, 2368 (2021).

64. Chatzantoni, K. & Mouzaki, A. *Anti-TNF-α Antibody Therapies in Autoimmune Diseases*. *Curr. Top. Med. Chem.* **6**, 1707-1714 (2006).

65. Brynskov, J., Foegh, P., Pedersen, G., Ellervik, C., Kirkegaard, T., Bingham, A., & Saermark, T. Tumour necrosis factor α converting enzyme (TACE) activity in the colonic mucosa of patients with inflammatory bowel disease. *Gut* (www.gutjnl.com) **51**, 37-43 (2002).

66. Beromun EMA information. https://www.ema.europa.eu/en/medicines/human/EPAR/beromun

67. Maney, N. J., Reynolds, G., Krippner-Heidenreich, A. & Hilkens, C. M. U. Dendritic Cell Maturation and Survival Are Differentially Regulated by TNFR1 and TNFR2. *J. Immunol.* **193**, 4914–4923 (2014).

68. Hubo, M., Trinschek, B., Kryczanowsky, F., Tuettenberg, A., Steinbrink, K., & Jonuleit, H. Costimulatory molecules on immunogenic versus tolerogenic human dendritic cells. *Front. Immunol.* **4**, 82 (2013).

69. Armendáriz-Barragán, B., Zafar, N., Badri, W., Galindo-Rodríguez, S. A., Kabbaj, D., Fessi, H., & Elaissari, A. Plant extracts: from encapsulation to application. *Expert Opin. Drug Deliv.* **13**, 1165–1175 (2016).

70. Kalani, M. & Yunus, R. Application of supercritical antisolvent method in drug encapsulation: a review. *Int. J. Nanomed.* **6,** 1429–1442 (2011).

71. Bruschi, M. L. Main mechanisms to control the drug release. Strategies to Modify the Drug Release from Pharmaceutical Systems. *Woodhead Publishing: Cambridge, UK*, 37–62 (2015). doi:10.1016/b978-0-08-100092-2.00004-7.

72. Siegel R. A., Rathbone M. J. Overview of controlled release mechanisms. In: *Fundamentals and Applications of Controlled Release Drug Delivery*. Springer US; 2012:19-43. doi:10.1007/978-1-4614-0881-9_2

73. Ciriminna, R., Fidalgo, A., Pandarus, V., Beland, F., Ilharco, L. M., & Pagliaro, M. The sol-gel route to advanced silica-based materials and recent applications. *Chem. Rev.* **113**, 6592–6620 (2013).

74. Shin, H. S., Hwang, Y. K. & Huh, S. Facile preparation of ultra-large pore mesoporous silica nanoparticles and their application to the encapsulation of large guest molecules. *ACS Appl. Mater. Interf.* **6**, 1740–1746 (2014).

75. Beganskienė, A., Sirutkaitis, V., Kurtinaitienė, M., Juškėnas, R. & Kareiva, A. *FTIR, TEM and NMR Iinvestigations of Stöber Silica Nanoparticles*. *Mater. Sci*. **10** (4) 287-290 (2004).

76. Thommes, M., Kaneko, K., Neimark, A. V., Olivier, J. P., Rodriguez-Reinoso, F., Rouquerol, J., & Sing, K. S. Physisorption of gases, with special reference to the evaluation of surface area and pore size distribution (IUPAC Technical Report). *Pure Appl. Chem.* **87**, 1051–1069 (2015).

77. Tang, F., Li, L. & Chen, D. Mesoporous silica nanoparticles: Synthesis, biocompatibility and drug delivery. *Adv. Mater.* **24**, 1504–1534 (2012).

78. Deng, Y., Qi, D., Deng, C., Zhang, X. & Zhao, D. Superparamagnetic high-magnetization microspheres with an Fe3O4@SiO2 core and perpendicularly aligned mesoporous SiO2 shell for removal of microcystins. *J. Am. Chem. Soc.* **130**, 28–29 (2008).

79. Li, W., Mayo, J. T., Benoit, D. N., Troyer, L. D., Lewicka, Z. A., Lafferty, B. J., Catalano, J. G., Lee, S., Colvin, V. L. & Fortner, J. D. Engineered superparamagnetic iron oxide nanoparticles for ultra-enhanced uranium separation and sensing. *J. Mater. Chem. A* **4**, 15022–15029 (2016).

80. Adan, A., Alizada, G., Kiraz, Y., Baran, Y. & Nalbant, A. Flow cytometry: basic principles and applications. *Crit. Rev. Biotechnol.* **37**, 163–176 (2017).

81. Eskandari, M., Nguyen Kunkel, D. S. & Remick, D. *WEHI 164 subclone 13 assay for TNF: sensitivity, specificity, and reliability. Immunol. Invest.* **19** (1), 69-79 (1990).

82. abcam protocols book.

https://docs.abcam.com/pdf/misc/abcam-protocols-book.pdf

83. Lokras, A., Thakur, A., Wadhwa, A., Thanki, K., Franzyk, H., & Foged, C. Optimizing the Intracellular Delivery of Therapeutic Anti-inflammatory TNF-α

siRNA to Activated Macrophages Using Lipidoid-Polymer Hybrid Nanoparticles. *Front Bioeng. Biotechnol.* **8**, 1538 (2021).

84. Auría-Soro, C., Nesma, T., Juanes-Velasco, P., Landeira-Viñuela, A., Fidalgo-Gomez, H., Acebes-Fernandez, V., & Fuentes, M. (2019). Interactions of nanoparticles and biosystems: Microenvironment of nanoparticles and biomolecules in nanomedicine. *Nanomaterials* **9**, 1365 (2019).

85. Cosgrove, T., Crowley, T. L., Ryan, K. & Webster, J. R. P. *The effects of solvency on the structure of an adsorbed polymer layer and dispersion stability*. *Coll. Surf.* **51,** 255-269 (1990).

86. Macha, I. J., Ben-Nissan, B., Vilchevskaya, E. N., Morozova, A. S., Abali, B. E., Müller, W. H., & Rickert, W. Drug delivery from polymer-based nanopharmaceuticals-an experimental study complemented by simulations of selected diffusion processes. *Front. Bioeng. Biotechnol.* **7**, 37 (2019).

87. Park, C. G., Hartl, C. A., Schmid, D., Carmona, E. M., Kim, H. J., & Goldberg, M. S. *Park et al Extended release of perioperative immunotherapy prevents tumour recurrence and eliminates metastases*. *Sci. Transl. Med.* **10,** eaar1916 (2018).

88. Lim, J. W., Na, W., Kim, H. O., Yeom, M., Park, G., Kang, A., Chun, H., Park, C., Oh, S., Le, V. P., Jeong, H. H., Song, D. & Haam, S. Cationic Poly(Amino Acid) Vaccine Adjuvant for Promoting Both Cell-Mediated and Humoral Immunity Against Influenza Virus. *Adv. Healthcare Mater.* **8**, 1800953 (2019).

89. Jonuleit, H., Kühn, U., Müller, G., Steinbrink, K., Paragnik, L., Schmitt, E., & Enk, A. H. Pro-inflammatory cytokines and prostaglandins induce maturation of potent immunostimulatory dendritic cells under fetal calf serum-free conditions. *Eur. J. Immunol*. **27** (12), 3135-3142 (1997).

90. Zhang, L. W., Bäumer, W. & Monteiro-Riviere, N. A. Cellular uptake mechanisms and toxicity of quantum dots in dendritic cells. *Nanomedicine* **6**, 777–791 (2011).

91. Tomić, S., Đokić, J., Vasilijić, S., Ogrinc, N., Rudolf, R., Pelicon, P., & Čolić, M. Size-dependent effects of gold nanoparticles uptake on maturation and

antitumor functions of human dendritic cells in vitro. *PLoS ONE* **9**, e96584 (2014).

92. Ashley, C. E., Carnes, E. C., Phillips, G. K., Padilla, D., Durfee, P. N., Brown, P. A. & Brinker, C. J. The targeted delivery of multicomponent cargos to cancer cells by nanoporous particle-supported lipid bilayers. *Nature Mater.***10**, 389–397 (2011).

93. Ferrari, Mauro. Beyond drug delivery. *Nature Nanotechnol*. **3** (3), 131-132 (2008).

94. Deming, T. J. Synthesis of Side-Chain Modified Polypeptides. *Chem. Rev.* **116** 786–808 (2016).

8 List of Figures

9 List of Tables

10 List of Abbreviations

DDSs: drug delivery systems

NPs: nanoparticles

FDA: food and drug administration (USA)

TNF-α: tumour necrosis factor-alpha

DCs: dendritic cells

APCs: antigen presenting cells

MHC: major histocompatibility complex molecules

PAMPs: pathogen-associated molecular patterns

DAMPs: danger-associated molecular patterns

Th: T helper

Mo-DCs: monocyte-derived DCs

PLGA: poly(lactic-co-glycolic acid)

PEG: polyethylene glycol

pSi: porous silicon

MSNs: mesoporous silica nanoparticles

IgGs: Immunoglobulins

PVA: polyvinyl alcohol

GMP: good manufacturing practices

PEI: polyethyleneimine

FUCCI: fluorescent ubiquitination-based cell cycle indicator

P-L-L: poly-l-lysine

MET: micro-emulsion templating approach

TEOS: tetraethylorthosilicate

PS: polystyrene

NK cells: natural killer cells

IBD: inflammatory bowel disease

STS: soft tissue sarcoma

ILP: isolated limb perfusion

CTAC: cetyltrimethylammonium chloride

TEA: triethanolamine

PBS: phosphate-buffered saline

TEM: transmission electron microscopy

DLS: dynamic light scattering

CF300-CU: carbon film supported copper square mesh size 300

BJH: Barrett-Joyner-Halenda

BET: Brunauer-Emmett-Teller

NMR: nuclear magnetic resonance

ATR-FTIR: attenuated total reflection Fourier-transform infrared spectroscopy

MTT: 3-(4,5-dimethylthiazol-2-yl)-2,5-diphenyltetrazolium bromide

DMSO: dimethyl sulfoxide

ELISA: enzyme-linked immunosorbent assay

DMEM: Dulbecco's modified Eagle's medium

FCS: fetal calf serum

RPMI: Roswell park memorial institute

EDTA: ethylenediaminetetraacetic acid

Pen Strep: penicillin-streptomycin

HSA: human serum albumin

rh: recombinant human

PGE_2: prostaglandin E_2

FITC: fluorescein isothiocyanate

PE: phycoerythrin

PBMCs: peripheral blood mononuclear cells

GM-CSF: granulocyte-macrophage colony-stimulating factor

IL: interleukin

HLA-DR: human leukocyte antigen – DR isotype

MLR: mixed lymphocyte reaction

$DMSN_{OPT}$: dendritic mesoporous silica nanoparticle optimal

SAED: selected area electron diffraction

MS: magnetic separation

EDX: energy dispersive X-ray spectroscopy

7-AAD: 7-Aminoactinomycin D

DNA: deoxyribonucleic acid

SSC: side scatter

FSC: forward scatter

LPNs: lipidoid-polymer hybrid nanoparticles

SN: supernatant

Sar-Lys: sarcosine-lsyine

PDI: polydispersity Index

pH: power of hydrogen

SD: standard deviation

MFI: mean fluorescence intensity

cpm: counts per minute

^{3}H-Tdr: ^{3}H-thymidine

SLB: supported lipid bilayer

HEPES: 4-(2-hydroxyethyl)-1-piperazineethanesulfonic acid

LPS: lipopolysaccharide

TLR: toll-like receptor

QDs: quantum dots

BBB: blood-brain barrier

11 Curriculum Vitae: Kimia Rahmani